2016

Decitabine-loaded Nanogel Treatment to Reverse Cancer Drug Resistance

Samantha A. Cramer

DECITABINE-LOADED NANOGEL TREATMENT TO REVERSE CANCER DRUG RESISTANCE

SAMANTHA A. CRAMER

Bachelor of Science in Agricultural and Biological Engineering

Purdue University

December, 2008

Submitted in partial fulfillment of requirements for the degree

MASTER OF SCIENCE IN BIOMEDICAL ENGINEERING

at the

CLEVELAND STATE UNIVERSITY

May, 2016

We hereby approve this thesis for

Samantha A. Cramer

Candidate for the Master of Science in Biomedical Engineering degree for the

Department of Chemical and Biomedical Engineering

and the CLEVELAND STATE UNIVERSITY

College of Graduate Studies

Thesis Chairperson, (V. Labhasetwar)

Department & Date

Thesis Committee Member, (J. Belovich)

Department & Date

Thesis Committee Member, (C. Kothapalli)

Department & Date

Student's Date of Defense: (May 5, 2016)

DEDICATION

To my husband, James. For encouraging me to pursue my dreams and supporting me during this journey. I am very grateful.

ACKNOWLEDGEMENTS

I am grateful to my mentor, Dr. Vinod Labhasetwar, for giving me an opportunity to work under his guidance, and for his support, expertise, and encouragement throughout my graduate education. I believe his emphasis on precise writing and critical thinking will help me grow as a scientist.

I am thankful to Dr. Belovich and Dr. Kothapalli, for their significant contribution in my graduate studies including courses, meetings, and their helpful advice towards the completion of my research.

I am also thankful to everyone in Dr. Labhasetwar's lab for their help, encouragement, and support every day. I would specifically like to thank Dr. Isaac Adjei for teaching me how to be a scientist and for his patience and friendship. I am so lucky to have Melinda Stees in the lab every day for guidance, instructions, venting, and working through many issues together over the years.

This study was supported by a grant from the National Cancer Institute of the National Institutes of Health [Grant 1R01CA149359 (to V.L.)].

DECITABINE-LOADED NANOGEL TREATMENT

TO REVERSE CANCER DRUG RESISTANCE

SAMANTHA A. CRAMER

ABSTRACT

Cancers in which epigenetic changes, such as hypermethylation of DNA, lead to drug resistance cause the cancer to become unresponsive to existing chemotherapeutic treatments. The epigenetic drug – 5-aza-2'-deoxycytidine (decitabine, DAC) – is a potent hypomethylating agent, but its effect is transient due to its instability. Previous studies have shown that loading DAC into nanogel significantly enhances its antiproliferative effect (compared to DAC in solution) in drug-resistant breast cancer cells (MCF-7/ADR). Further, the previous studies demonstrated changes in the membrane lipid profile of resistant cells following treatment with DAC either as solution or in nanogels. The objective of the present study was to compare the stability of DAC as solution and DAC encapsulated in nanogel, determine the effect of duration of DAC and DAC-nanogel pretreatment on the antiproliferative activity of subsequent chemotherapeutic agent addition, and to visualize and quantify the effect of DAC and DAC-nanogel pretreatment on uptake of poly dl-lactide *co*-glycolide (PLGA)-based nanoparticle in MCF-7/ADR cells. An increase in the stability of DAC when encapsulated in nanogel could be a mechanism contributing to the sustained effect of DAC. DAC-nanogel's sustained effect and its effectiveness at altering the membrane lipid profile to reduce resistance could cause a longer DAC-nanogel pretreatment time to increase the antiproliferative effect of subsequent chemotherapeutic agent addition. Additionally, the membrane lipid profile altering effects of DAC and DAC-nanogel could cause DAC and DAC-nanogel

pretreatment to increase uptake of nanoparticles in MCF-7/ADR cells. The stability of DAC was assessed in mouse plasma at physiological conditions using mass spectrometry. DAC in solution was found to be less stable than DAC in nanogel. The effect of durations of 3-days and 5-days of DAC-nanogel treatments on the subsequent efficacy of chemotherapeutic agent, paclitaxel was assessed in MCF-7/ADR cells using a MTS assay. The DAC-nanogel had a greater effect with a longer duration of pretreatment time as determined by the dose-response curve, IC_{50}, and IC_{70}. The effect of DAC or DAC-nanogel pretreatment of a 3-day duration on subsequent uptake of nanoparticles was visualized with confocal microscopy and the differences in uptake were quantified. Increase in uptake of nanoparticles was seen in both DAC and DAC-nanogel with DAC alone having a greater effect. Overall, this study shows that increased DAC stability is a contributing factor to the increased efficacy and sustained effect of DAC-nanogel, the effect of DAC-nanogel on subsequent anticancer drug antiproliferative activity is significantly increased with a longer duration of pretreatment, and DAC and DAC-nanogel pretreatment cause a greater uptake of subsequent nanoparticle addition than in cells without any pretreatment.

TABLE OF CONTENTS

LIST OF TABLES

LIST OF FIGURES

CHAPTER I

INTRODUCTION

1.1 Introduction

Once cancer acquires drug resistance, it is difficult to treat with existing chemotherapeutics (Solyanik 2010). There are certain changes that cause cancer cells to become drug-resistant and exhibit characteristics that do not appear in drug-sensitive cancer cells. One of these characteristics is reduced drug transport into resistant cells due to changes in the membrane lipid composition leading to greater membrane rigidity than that of sensitive cell membrane (Peetla et al. 2010). Another characteristic is that drugs that are transported across the membrane are then trapped in endosomal vesicles so that they are not available for interaction with intracellular targets, or they are trapped in the membrane but then effluxed out from the cell via permeability glycoprotein (P-gp) which is over-expressed in resistant cells. These events, increased rigidity of the cell membrane, endosomal entrapment, and increased efflux by P-gp lead to impaired drug transport or endocytosis that affects nanocarrier-mediated drug delivery and cause chemotherapeutic agents to be less effective (Gottesman 2002; Peetla et al. 2013).

The acquired drug resistance seen in some cancers is due to epigenetic changes to the genome (Knappskog and Lønning 2012). These changes affect the expression of the genes without altering the DNA sequence. 5-aza-2'-deoxycytidine (decitabine [DAC]), a hypomethylating agent, reactivates silenced genes. DAC treatment achieves hypomethylation via covalent binding of DNA methyltransferase 1 (DNMT1) (Onda et al. 2012). This results in a decrease in the amount of DNMT1 available to carry out methylation. Although the demethylation and reactivation of tumor suppressor genes is often the primary focus of DAC research, another effect of the hypomethylation is that it causes the lipid profile of the cell membrane to be altered by means of altered membrane lipid synthesis (Vijayaraghavalu et al. 2012).

The resistant cells treated with DAC have membrane lipid profiles that resemble more or less that of a sensitive cell's lipid profile. When these DAC-treated resistant cells are then sequentially treated with anti-cancer drug, the anti-cancer drug's efficacy is enhanced (Vijayaraghavalu et al. 2012). The benefit of using DAC in this manner – as a pretreatment – is that although *in vitro* DAC is an effective antiproliferative agent by itself, *in vivo* it becomes toxic at higher doses (especially in bone marrow) due to its DNA-damaging activity and targeting rapidly dividing bone marrow cells, causing myelosuppression (Hollenbach et al. 2010). DAC has a significantly short half-life (10 – 35 minutes *in vivo*) because of its rapid clearance rate as it has low affinity for plasma proteins, and it is also rapidly degraded by cytidine deaminase in the liver (Jabbour et al. 2008).

The efficacy of pretreatment with DAC could be improved upon by overcoming some of the factors that have limited its use in clinical trials. Currently, DAC is approved by the FDA as a monotherapeutic agent to treat hematological cancers (Boumber and Issa 2011). Treatment of solid tumors with DAC has been attempted in clinical trials with disappointing results (Boumber and Issa 2011). There are several factors that limit the performance of DAC in solid tumors, as it cannot achieve therapeutic dose because of short half-life and repeated and high dosing of DAC to maintain therapeutic level at the tumor site causes myelosuppression and leukopenia (Momparler et al. 1997). Loading DAC into nanogel has been shown to significantly enhance its antiproliferative effect in drug-resistant breast cancer cells (MCF-7/ADR) due to prolonged DNMT1 depletion (Vijayaraghavalu and Labhasetwar 2013). In aqueous solutions and culture media DAC rapidly degrades due to hydrolytic opening of the 5-azacytosine ring resulting in many degradation products (Stresemann and Lyko 2008; Rogstad, D. K. et al. 2009). The sustained effect may be due to the nanogel increasing DAC stability in culture medium. In addition to a greater efficacy of DAC, nanogel confers other properties useful in overcoming difficulties associated with using DAC *in vivo*. Nanogel can potentially reduce this toxicity because nanogel may not be able to pass through the openings in the sinusoidal capillaries of bone marrow as freely as drug molecules. DAC-nanogel could protect DAC from deamination by cytidine deaminase in the liver, spleen, and plasma (Stresemann and Lyko 2008). Another benefit of nanogel is that DAC's method of action is S-phase dependent. Tumor cells have been shown to divide at a slower pace *in vivo* versus *in vitro.* The sustained effect of DAC-nanogel could expose cancer cells at the

tumor site to DAC for a longer duration so that the DAC can be incorporated into the DNA when the cancer cells go through S-phase (Brünner et al. 1989; Oloumi et al. 2010).

1.2 Hypothesis

It is hypothesized that DAC is more stable when loaded in nanogel, that this stability means the duration of DAC-nanogel pretreatment will correlate with its ability to increase subsequent drug efficacy, and that DAC-nanogel pretreatment will cause a greater uptake of nanoparticles in drug resistant breast cancer cells (MCF-7/ADR).

1.3 Specific Aims

1. One aim of this research was to test the stability of DAC alone versus DAC-nanogel by comparison in plasma under physiological conditions over time using high pressure liquid chromatography (HPLC), UV/VIS, and mass spectroscopy.

2. A second aim was to determine how duration of pretreatment with DAC and DAC-nanogel affects the anti-proliferative effect of subsequent chemotherapeutic drug treatment in drug resistant breast cancer cells. MCF-7/ADR cells were treated with DAC alone, DAC-nanogel, or control, with durations of three or five days. All samples were then treated with chemotherapeutic agent and dose response curves, IC_{50}s, and IC_{70}s (concentration of the drug which causes 50% or 70% inhibition of cell growth) were obtained using MTS assays.

3. A final aim was to assess nanoparticle uptake in MCF-7/ADR cells after pretreating with DAC, DAC- nanogel, or no pretreatment. Nanoparticles loaded with 6-coumarin dye were added to the pretreated cells. The cells were imaged with confocal

microscopy. The amount of nanoparticle uptake per cell was quantified using the intensity of the green 6-coumarin dye.

1.4 Significance of Research

The stability of DAC-nanogel versus DAC alone will be helpful information for planning the specifics of using DAC- nanogel *in vivo*. Greater stability would mean a longer retention time *in vivo*. The stability could be a part of the mechanism of action accounting for the increased effectiveness.

Additional information on the mechanism that would aid *in vivo* study set-up is the effect of the duration of pretreatment with DAC on uptake of subsequent anticancer drug. Confocal microscopy of dye-loaded nanoparticles will be used to visualize and quantify differences after pretreatment with DAC and DAC-nanogel on cellular uptake of the dye-loaded nanoparticles. The resulting images will show the amount of dye-loaded nanoparticles inside the cells indicating the amount of endocytosis. The principle of increased uptake from increased endocytosis of dye-loaded nanoparticles could be expanded in theory to include uptake of drug or drug-loaded nanoparticles.

Taken together, this research could further the case for using DAC-nanogel as a pretreatment for drug-resistant cancers. It also elucidates on the mechanism of action – greater stability and increased uptake by the cell membrane – by which the pretreatment is improving efficacy.

CHAPTER II

BACKGROUND

2.1 Cancer Drug Resistance and Epigenetics Role

Drug resistance is a major problem in cancer chemotherapeutics and a multifactorial phenomenon. The resistance may be preexisting within the genetic code of the cancer cells, or the resistance may be acquired after treatment with chemotherapeutics (Solyanik 2010). There are mechanisms of resistance that reduce the amount of drug within the cell via decreased drug influx, drug sequestration in intracellular vesicles, and increased drug efflux by way of P-glycoprotein (P-gp) (also known as multidrug resistance [MDR] protein 1) pumps. Other mechanisms change the apoptotic cell pathways to avoid cell death (Gottesman 2002; Pérez-Tomás 2006). Cancers that acquire drug resistance may do so through genetic changes to the genome. An example of acquired resistance through genetics is the mutation of the gene for p53 which causes a decrease in apoptosis (Knappskog and Lønning 2012).

Epigenetics is a change in the genetic activity without changing the nucleotide sequence. Mechanisms of epigenetic regulation include DNA methylation, chromatin remodeling (histone modification), small interfering RNA (siRNA) and micro RNA

(miRNA) – mediation (Nakao 2001; Bird 2007; Goldberg et al. 2007). Methylation – methyl group addition to DNA - is known for its gene silencing effect but can also regulate imprinting and X-chromosome inactivation. DNA methyltransferase (DNMT) is the enzyme responsible for methylation in mammal genomes. DNMT adds methyl groups to clusters of cytosine and guanine near gene promoters (termed CpG islands) or to histone amino acids, affecting gene expression (Jones and Takai 2001; Jones 2012). The role of methylation in acquired drug resistance in cancer has been extensively studied. There is an increase in methylation (hypermethylation) of promoters of several tumor suppressor genes such as retinoblastoma tumor-suppressor gene (*Rb*) and breast cancer type 1 susceptibility protein (*BRCA1*) (Esteller 2007). Hypomethylation is also seen in acquired drug resistant in genes that prevent apoptosis and enhance cell survival (Gopisetty et al. 2006).

2.2 Approaches for Overcoming Resistance

Significant effort has been devoted to overcoming drug resistance primarily focusing on drug transport. A thoroughly investigated family of transporters that cause increased efflux of drug with low specificity is the ATP-binding cassette (ABC) transporter family, of which the P-gp pump is a member. There are drugs which shut down the P-gp efflux pump and often these are used in combination with an anticancer drug to act synergistically (Szakács et al. 2006; Peetla et al. 2013). Combinations of multidrug – resistance gene silencers made up of siRNA or miRNA or with anticancer drug have also been investigated (Peetla et al. 2013).

There are several drugs that target epigenetic mechanisms currently in preclinical or clinical trials or approved for use. Of particular interest is decitabine (DAC), which has a molar mass of 228.21 g/mol and a molecular formula of $C_8H_{12}N_4O_4$ (Neupane, Y. R. et al. 2015) . DAC is an analog to the nucleoside cytidine (shown in **Figure 1a**) and therefore exploits the same metabolic pathway (Jordheim et al. 2013). It crosses the membrane via the human equilibrium nucleoside transporter 1 (hENT1) protein (Damaraju et al. 2012). Intracellularly, it is converted to its active form – DAC triphosphate – then incorporates into the DNA during S-phase as shown in **Figure 1b** (Jordheim et al. 2013). When DNMT attempts to methylate the daughter strand of DNA in which the DAC has been incorporated in place of cytidine, DNMT is irreversibly bound to DAC and degraded. Normally, a nucleophilic attack initiates DNMT's methylation of the substrate cytidine, methylation occurs, and the bond is broken by beta-elimination at the carbon-5 atom. The nitrogen atom at position 5 of DAC causes an unresolvable covalent bond to occur between DNMT and the carbon at position 6 of the DAC. This triggers a DNA damage response and the DNMT is targeted for proteosomal degradation (Stresemann and Lyko 2008; Yang et al. 2010). Initially, the result is hemimethylated DNA as shown in **Figure 1c**. In subsequent round of replication the DNMT remains depleted and the DNA becomes increasingly hypomethylated (Santini et al. 2001). This hypomethylation of the DNA results in reactivation of silenced genes such as tumor suppressor genes (Cramer et al. 2015).

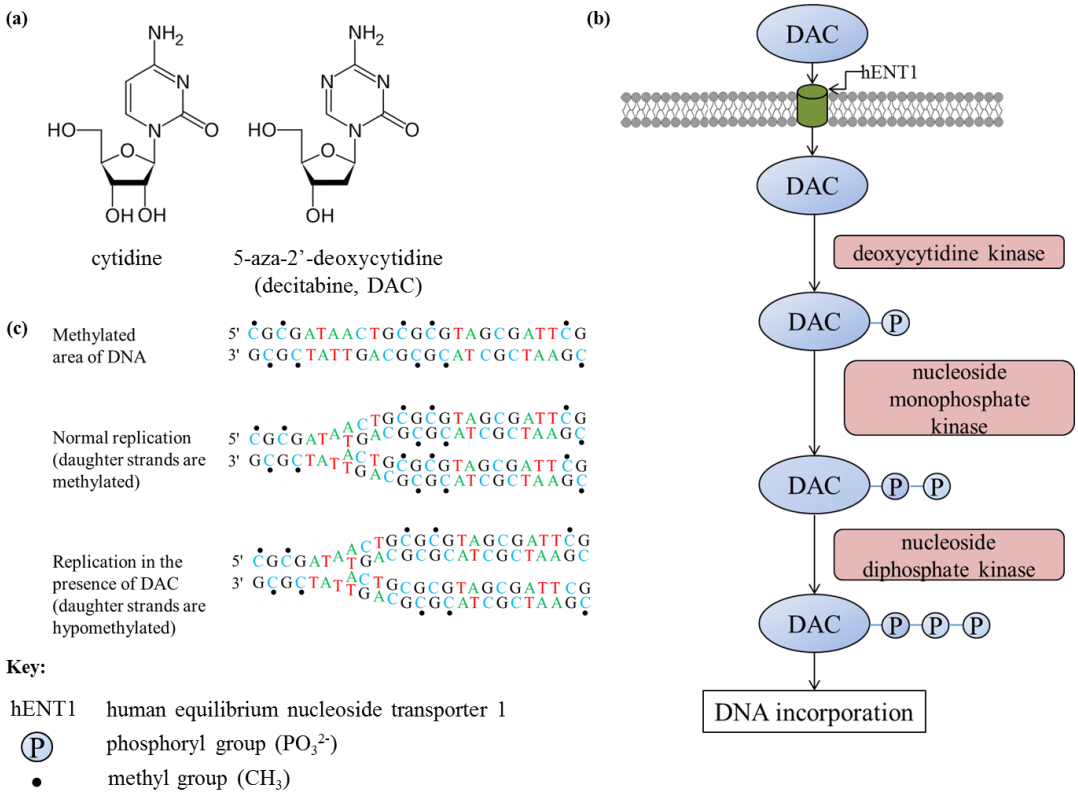

Figure 1: Molecular structure, metabolic pathway, and hypomethylation action of decitabine (DAC). (a) The molecular structure of cytidine and DAC. The key difference is the 5-carbon of cytidine being replaced by nitrogen in DAC. (b) DAC enters the cell through the human equilibrium nucleoside transporter 1 (hENT1). It is subsequently phosphorylated by deoxycytidine kinase, nucleoside monophosphate kinase, then nucleoside diphosphate kinase to form DAC-triphosphate which is incorpoarated into DNA during S-phase. (c) Some deoxycytidylate-phosphate-deoxyguanylate (CpG) islands are methylated (the addition of CH_3 represented her by addition of a • to cytosine) in the initial DNA. During normal replication, DNMT maintains methylation by addition of methyl groups to the newly formed daughter strand symmetrically. In the presence of DAC, DNMT is depleted leading to the DNA in the daughter cells being hemimethylated. Subsequent rounds of DNA replication in the absence of DNMT will lead to increasingly hypomethylated DNA. Figure 1a decitabine molecule is from (Fvasconcellos 2007).

At high doses, which are necessary to achieve therapeutic levels in solid tumors, DAC is toxic, especially to the rapidly dividing cells in the bone marrow, and can cause chronic myelosuppression and leukopenia. The mechanism of toxicity is DAC's DNA

damaging activity, replacing cytidine in the replicating cell, and not its hypomethylation activity (Brown and Plumb 2004).

DAC has been successful in clinical trials against hematologic malignancies (tumors that affect the blood, bone marrow, lymph, and lymphatic system). DAC is approved for use in the treatment of myelodysplastic syndrome (MDS). It is also used off-label to treat acute myeloid leukemia (AML) in the elderly and in a phase III trial. But, the efficacy of DAC in treating solid tumors has been disappointing. This is due to the difference in the pharmacokinetics and pharmacodynamics in between solid tumors and hematological malignancies. In acidic conditions, DAC degrades due to cleavage of the glycosidic bond. In basic and neutral aqueous conditions such as those *in vitro* studies, the opening of the 5-azacytosine ring is the cause of the degradation (Stresemann and Lyko 2008). *In vivo*, characteristics such as a very high clearance rate (half-life of 10-35 min), rapid degradation in acidic environment such as those in solid tumors (due to cleavage of the glycosidic bond), and rapid degradation by cytidine deaminase (found principally in the liver) come into play (Jabbour et al. 2008). Also, as DAC is S-phase dependent, its efficacy in solid tumors could be affected by the slower dividing of cancer cells *in vivo* versus *in vitro* (Momparler et al. 1997). It may take 5-15 days for all the cells in a tumor to pass through S-phase (Brünner et al. 1989; Oloumi et al. 2010).

2.3 Lipid Biosynthesis in Drug Resistant Cells and Alteration with DAC

Altered lipid makeup of the cell membrane can be a characteristic of drug resistant cells (Escribá et al. 2008). Recent studies have shown that in breast cancer drug resistant cells (MCF-7/ADR) the lipid profile of the cell membrane is a mechanism of

drug resistance and the lipid synthesis is epigenetically controlled (Peetla et al. 2010; Vijayaraghavalu et al. 2012). The makeup of the membrane in these cells influences drug transport or endocytosis for nanoparticle-mediated drug delivery. Peetla et al. compared a breast cancer cell line with acquired resistance - MCF-7/ADR - to the sensitive breast cancer cell line – MCF-7 (Peetla et al. 2010). The resistant cells had more sphingomyelin (SM), phosphatidylinositol, cholesterol, and cholesterol esters leading to a more rigid, compact, and hydrophobic membrane (Peetla et al. 2010). When anticancer drug (doxorubicin) was added to the cells, it was seen that the greater hydrophobic makeup of the resistant cell membrane led to sequestration of the drug in the membrane, therefore less drug got into the cell. The intracellular concentration of anticancer agent required for an antiproliferative effect was the same in resistant and sensitive cells (Peetla et al. 2010). This supports the claim that it is the reduced uptake in the resistant cells that is a part of the source of resistance. Membrane lipid alterations are known to occur concurrently with most known drug-resistance mechanisms (Pallarés-Trujillo et al. 2000; Hendrich and Michalak 2003).

The changes seen in the lipid profile of resistant cells could be due to numerous influences, one of which could be hypermethylation of one or multiple genes implicated in cell membrane protein/lipid synthesis (Vijayaraghavalu et al. 2012). The sphingomyelinase (SMase) gene has been seen to be hypermethylated in 60% of breast tumors. SMase hydrolyzes SM to become ceramide – a lipid with tumor suppression functions and the ability to take the place of cholesterol in the cell membrane. Decreased cholesterol in the membrane leads to greater fluidity. When treated with DAC, this SMase gene is re-expressed (Demircan et al. 2009).

Studies have shown that DAC treatment can reverse some of the changes in the lipid composition and biophysical characteristics of the membrane of resistant cells, causing an increase in drug sensitivity (Vijayaraghavalu et al. 2012; Peetla et al. 2013). The lipid composition of the membrane of resistant cells treated with DAC displayed increased SMase activity, thus decreasing the amount of SM in the membrane. SM, cholesterol, and P-gp activity are interdependent (Slotte and Bierman 1988; Vijayaraghavalu et al. 2012). Thus, P-gp expression was also seen to decrease and fluidity of the membrane was increased. The biophysics and endocytic function of resistant cells resembled that of the sensitive cells after DAC treatment and drug efficacy was enhanced (Vijayaraghavalu et al. 2012; Peetla et al. 2013).

2.4 DAC-Nanogel

DAC has several characteristics that limit its use *in vivo* as discussed previously. Hydrophilic drugs, such as DAC, can be loaded into hydrophilic nanogels at a higher drug-loading capacity than other forms of drug delivery such as nanoparticles, polymeric micelles, or liposomes. A nanogel is a nano-sized hydrogel (usually tens to hundreds of nanometers in diameter) composed of hydrophilic polymer chains which are physically or chemically cross-linked (Kabanov, A. V., & Vinogradov, S. V. 2009). It has been shown that when DAC is loaded into a biodegradable N-isopropylacrylamide (NIPAM) based nanogel its efficacy is increased compared to treatment with DAC alone in MCF-7/ADR cells (Vijayaraghavalu and Labhasetwar 2013). This NIPAM –based nanogel has been thoroughly studied for loading with DAC and the materials and methods used for the synthesis, loading, and characterization of the DAC-nanogel have been optimized in previous studies. The DAC is released from this nanogel due to biodegradation of the

nanogel. In the previous study, the DAC-nanogel diminished the transient nature of DAC via more sustained DNMT1 depletion and prolonged cell cycle arrest in the G2/M phase. The mechanism behind the sustained effect may be an increase in the stability of DAC when it is loaded into the nanogel. This hypothesis is tested in the first aim of the research herein. Instead of comparing the efficacy of DAC and DAC-nanogel as a primary treatment, the second aim of the research herein compares DAC and DAC-nanogel as varying durations of pretreatments and calculates the effect by subsequent response to antiproliferative drug treatment. Void (empty) nanogel was not used as a control because it has shown no cytotoxicity in previous studies (Vijayaraghavalu and Labhasetwar 2013). Another previous study – similar to the study showing that DAC alone causes resistant cell's lipid profile to resemble that of a sensitive cell – showed that DAC-nanogel was even more effective than DAC alone in causing this change in the lipid profile (Raghavan et al. 2015). The third aim of the research herein builds on the previous research by again using DAC and DAC-nanogel but comparing their effects on subsequent uptake of nanoparticles across the cell membrane.

CHAPTER III

MATERIALS AND METHODS

3.1 Materials

N-isopropylacrylamide (NIPAM), n-hexane, benzene, vinyl pyrrolidone (VP), sodium dodecylsulfate (SDS), sodium acrylate, N,N'-cystamine bisacrylamide, ammonium persulfate (APS), maleic anhydride, dimethyl sulfoxide (DMSO), 5-aza-2'-deoxycytidine (decitabine, DAC), Daidzin, and paclitaxel (PTX) were purchased from Sigma–Aldrich Chemical Company (St. Louis, MO). Poly(ethylene glycol) (PEG, M.W. ~5000) was purchased from Polysciences, Inc. (Warrington, PA). Cell culture media, Dulbecco's phosphate-buffered saline (DPBS), penicillin and streptomycin were purchased from the Central Cell Services Media Laboratory of the Lerner Research Institute. MTS reagent was purchased from Promega (Madison, WI). Mouse plasma was purchased from GeneTex Inc. (Irvine, CA).

3.2 DAC Solution

DAC (either 5 mg or 10 mg) was reconstituted to a concentration of 8.1 mg/mL by addition of DMSO (maximum solubility of DAC in DMSO is 20 mg/mL) then kept at

-20 °C in 100 µL aliquots. The stability of storing these aliquots for up to four months was confirmed through HPLC comparison with fresh stock. Upon use, the concentration of DMSO was always diluted to below 0.1% v/v. DAC was protected from light degradation in all experiments using aluminum foil or decreased lighting.

3.3 DAC Nanogel

3.3.1 Nanogel Synthesis

Nanogel was synthesized by surfactant polymerization of N-isopropylacrylamide (NIPAM) (700 mg) in the presence of PEG-maleic anhydride polymer (PEGMA) (100 mg), using vinyl pyrrolidone (VP) (200 mg) as a co-monomer, sodium dodecylsulfate (SDS) (200 mg) as a surfactant, ammonium persulfate (APS) (80 mg) as an initiator, and N,N′-cystamine bis(acrylamide) (60 mg) as a S-S cross-linker, at 70 °C for six hours, as previously described (Vijayaraghavalu and Labhasetwar 2013).

3.3.2 Loading Nanogel with DAC

Thirty mg of lyophilized nanogel was added to six mL MilliQ water in a 16 mL glass vial (Fisher Scientific, Pittsburgh, PA) and stirred slowly at room temp until dispersed. This was sonicated for five minutes at 20% amplitude using a Qsonica, LLC (Newtown, CT) Q500 with a 1/8” microtip. This time and amplitude have been optimized to achieve a low polydisperity index and to not create foam.

The dispersion was determined using a NICOMP™380 ZLS (Particle Sizing Systems, Santa Barbara, CA) by dynamic light scattering at a scattering angle of 90 º at

25 °C and zeta potential in the phase analysis mode and the current mode at a scattering angle of −14 °.

Three hundred µL of the 8.1 mg/mL aliquots of DAC (aliquoted in DMSO) was added in a dropwise fashion to the nanogel dispersed in water. This volume was with the goal of obtaining an 8% wt/wt solution of the DAC weight to the nanogel weight which has been determined to be optimal for loading. This was stirred for three hours in the cold room at 4 °C.

Next, the dialysis tubing (MWCO 12-kD, Spectrum Laboratories, Rancho Dominguez, CA) was prepared. The outside was wet to allow opening of the tubing. Once open, MilliQ water was run through the tubing. The tubing was then soaked in MilliQ water at a temperature of 85 - 90 °C for 30 min. This is done to remove the sodium azide preservative that may remain from the manufacturing process.

The dialysis of the DAC-loaded nanogel was performed against MilliQ water for 30 minutes in the cold room. This amount of time was determined by previous work to be sufficient to remove free DAC and DMSO. Next, the samples were frozen at -80 °C then lyophilized over two days at −48 °C, 3.5 Pa, using FreeZone 4.5 (Labconco Corp., Kansas City, MO). The lyophilized samples were stored at -20 °C.

3.3.3 Determination of DAC Loading in Nanogel

To determine the loading of the nanogel, the DAC was extracted back out of a small test sample. 2 mL MeOH was added to 1 mg of lyophilized DAC loaded nanogel in a 8 mL glass vial (Fisher Scientific, Pittsburgh, PA) and stirred overnight (12 hours) at 100 rpm in the cold room at 4 °C. 1 mL of the solution was taken into a 1.5 mL

Eppendorf tube and centrifuged at 14,000 rpm (Eppendorf 5417 R, Hauppauge, NY) for 10 min at 4 °C. DAC concentration in the supernatant was determined using HPLC (Shimadzu Scientific Instruments, Inc., Columbia, MD).

A standard plot of DAC (0 - 50 µg/mL) was prepared using the same conditions. Examples of standard curves from four different runs/days are shown in **Figure 2**. To be sure of the extent of extraction, the above protocol for loading was followed except the dialysis step was skipped so that all of the original DAC added to the nanogel should remain. It was determined that recovery was over 99% which is also reported in another study (Vijayaraghavalu and Labhasetwar 2013).

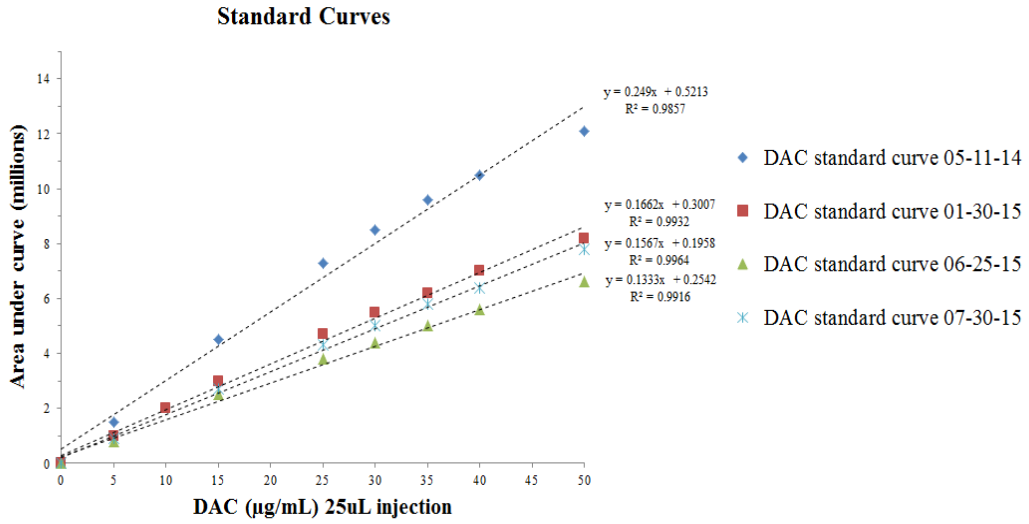

Figure 2: Standard HPLC curves of four different runs/days showing variability in area under the curve and demonstrating the need to create a new standard curve each time a loading concentration of DAC in nanogel is to be determined.

The HPLC conditions used to determine nanogel loading is described here. A C18 reversed phase column (Atlantis T3 –4.6 x 250 mm – 5 µm) was used with a mobile phase consisting of sterile degassed methanol:water (60:40 v/v). The injection volume was 25 µL. The flow rate was1.2 mL/min in isocratic mode for a total of six minute run

time per injection. The UV detection wavelength was 228 nm (Vijayaraghavalu and Labhasetwar 2013).

3.4 DAC Stability Analysis

3.4.1 Sample Preparation

Two mL mouse plasma samples (GeneTex Inc, Irvine, CA) in 8mL glass vials (Fisher Scientific, Pittsburgh, PA) were warmed to 37 °C in a MaxQ Mini 4450 Benchtop Incubated Orbital Shaker and kept rotating at 25 rpm. DAC solution, DAC-nanogel, or void nanogel was added to the plasma to achieve the desired concentration as shown in **Table 1**.

Sample	Concentration
DAC solution (high concentration)	100 µg/mL
DAC solution (low concentration)	300 ng/mL
DAC-nanogel	3 - 6 µg/mL
void nanogel	DAC-nanogel equivalent mass/volume

Table 1: Sample concentrations are shown for a high DAC solution concentration (*n* = 2), a low DAC solution concentration (*n* = 3), DAC-nanogel (*n* =4), and void (empty) nanogel (*n* = 2). All samples are in mouse plasma.

The high and low concentrations of DAC solution provide a range within which the DAC-nanogel stability curve can be compared to the DAC solution stability curve. These concentrations are discussed further in section 4.2. A sample of 200 µL was taken at timepoints 0, 1, 2, 4, and 8 hours and placed in cryovials and stored at -80 °C. Frozen samples were lyophilized as above (section 3.3.2) for two days.

3.4.2 Drug Extraction for Stability Curve Points

Before HPLC can be used to determine DAC concentration, the drug was extracted from the samples. This method is similar to the method of drug extraction in section 3.3.3 but instead of adding certain volume of methanol per weight, 200 µL methanol was added to each lyophilized sample to obtain the same concentration as the samples were previous to lyophilization. These were placed on an orbital shaker at 100 rpm in the cold room overnight. Next, the samples were vortexed vigorously and placed in the centrifuge at 13,200 rpm for 10 min at 4 °C. The supernatant (~100 µL) was collected in glass HPLC vials (Fisher Scientific, Pittsburgh, PA).

A liquid chromatography electrospray ionization tandem mass spectrometric method was developed (LC/ESI/MS/MS) for quantification of DAC in plasma using daidzin as internal standard. 20 µl of the sample (the supernatant from section 3.4.2) was injected onto a Waters HPLC (2690 Separations Module, Waters, Corp., Franklin MA, USA) and separated through a C18 column (2.1 x 150 mm, 5 µm, ODS, Phenomenex, Torrance, CA) using a gradient starting from 95% mobile phase A (water containing 5 mM ammonium acetate) at flow rate of 0.2 ml/min for 2 min, to 100% mobile phase B (acetonitrile containing 5 mM ammonium acetate) over 8 min and then with 100% B for 5 min as shown in **Table 2**.

time (min)	Mobile Phase
0-2	5% B
2-10	5% B to 100% B
10-15	100% B

Table 2: Mobile phase timeline for binary method in HPLC analysis of plasma samples.

The HPLC column effluent was introduced onto a Micromass triple quadrupole mass spectrometer (Quattro Ultima, Waters Inc., Beverly, MA) and analyzed using electrospray ionization in positive mode with multiple reaction monitoring (MRM). A potential difference of 3 keV was applied between the electrospray needle and the interior of the ion source. Hot nitrogen gas (250 °C) was used to help evaporating the solvent from the charged droplets and argon was used as the collision gas. The MRM transitions (m/z) were 457 → 113 for DAC and 417 → 255 for daidzin. The levels of decitabine in plasma were calibrated using internal standard daiazin. The assay was linear over the concentration range of 40 ng/mL -100 µg/mL. This method is adapted from published work. (Xu et al. 2012). Note that the HPLC/UV/VIS method was used for determination of loading and is described in section 3.3.3.

3.4.3 Stability Curves and Equations

The concentration data for the different timepoint samples of plasma were normalized for easier comparison and interpretation as the initial concentration (the zero hour timepoint) for each sample begins at 100% on the y-axis labeled '% DAC remaining'. Graphs of both absolute concentrations and the normalized data are shown in section 4.1.2. Normalization does not change the decay rate (K), just the Y_0 value. The data were fit to a one phase exponential decay model:

Equation 3.4: $$Y = (Y_0 - Y_{min})e^{-Kt} + Y_{min}$$

where Y_0 = the Y value when t (time) is zero, Y_{min} = the Y value at infinite time, and K is the rate constant. The half-life was computed as ln(2)/K. A paired two-tailed t test was also done to compute a p value and rule out the null hypothesis. The graph and calculations were done using GraphPad Prism 5.

3.5 Cell Culture

MCF-7/ADR cells (a gift from Dr. U. S. Rao's laboratory, Department of Biochemistry and Molecular Biology, University of Nebraska Medical Center) were maintained in Dulbecco's modified Eagle's medium (DMEM) supplemented with 15% fetal bovine serum (Gibco BRL, Grand Island, NY) and 100 µg/mL penicillin and 100 µg/mL streptomycin in 75 cm^2 culture flasks (BD Falcon, San Jose, CA). These conditions were optimized for growth of these cells. Drug resistance was maintained by culturing in media containing 100 ng/mL doxorubicin (Drug Source Co. LLC, Westchester, IL) after every two passages.

3.6 MTS Assay and IC_{50}/IC_{70} Calculations

3.6.1 Sample Setup

MCF-7/ADR cells were seeded at a density of 1.5 x 10^4 cells/mL in six 96-well plates (Lerner Research Institute, Cell Culture Services). Sixty wells per plate were seeded (all except the edge wells which were filled with PBS to prevent evaporation) with 100 µL media per well. After 24 hours cells were washed with PBS and treated with normal media, DAC solution, or DAC-nanogel at a concentration of 50 ng of DAC per mL of media. Three of the plates were incubated for 3 days at this stage (with normal

media, DAC, or DAC-nanogel) and three of the plates were incubated for 5 days at this stage (with normal media, DAC, or DAC-nanogel) as shown in **Table 3**.

Plate number	Pretreatment (DAC concentration for solution and nanogel is 50 ng/mL)
1	None (normal media) - 3 days
2	None (normal media) - 5 days
3	DAC solution - 3 days
4	DAC solution - 5 days
5	DAC-nanogel - 3 days
6	DAC-nanogel - 5 days

Table 3: Table showing setup for MTS assay. Each pretreatment type and duration is shown. Note that plate #4 (pretreatment type DAC solution with a duration of 5 days) was contaminated with fungus there are no results for this plate.

After the indicated pretreatment time (3 days or 5 days), cells were washed twice with PBS and 100 µL paclitaxel (PTX) in media was added at concentrations ranging from 0 – 20 µg/mL (0, 0.25, 0.50, 1, 2, 3, 4, 5, 10, and 20 µg/mL) and $n = 6$ for each concentration of PTX**.** Paclitaxel incubation time was 3 days for all plates. After this, cells were washed twice with PBS and normal media was added. After 2 days in normal media, MTS assays were performed.

3.6.2 Cytotoxicity Assay

An aliquot of 20 µL MTS reagent was added to each well, the plates were incubated for 2 hours at 37 °C, and color intensity was measured at 490 nm using a plate reader (Bio-Tek Instruments, Inc., Winooski, VT).

3.6.3 Dose Response Curves

Plate reader data was first transformed into logarithmic values then normalized so that the average of the six (n = 6) of the PTX concentration zero of each plate is the 100% growth point for that plate. Dose response curves were plotted on a semi-log graph.

3.6.4 IC_{50} and IC_{70} Calculations

To find the IC_{50}/IC_{70} values for each treatment type, first a variable slope line was fit to the data (already in log form) using this equation:

Equation 3.6 $$y = A_2 + \frac{A_1 - A_2}{1 + 10^{\log(x_0 - x)p}}$$

Where y = % cell growth (normalized), A_2 = % cell growth (normalized) at the bottom plateau region of the curve, A_1 = % growth at the top plateau region of the curve, x = PTX concentration, x_0 = the inflection point of the curve, and p = slope. To find the IC_{50}, y = 50. To find the IC_{70}, y = 70.

Two-way ANOVA statistical analysis was calculated for IC_{50}s and IC_{70}s comparing the no pretreatment to the DAC-nanogel treatments and determining if the duration of pretreatment was the cause of the significance (which is aim 2). This statistical analysis is discussed further in section 4.1.3 and detailed results from GraphPad Prism are in Appendix B.

3.7 Nanoparticle Uptake Study using Confocal Microscopy

3.7.1 Sample Preparation

MCF-7/ADR cells were seeded onto 35 mm glass bottom plates (MatTek Corp, Ashland, MA) at a density of 1.8 x 10^4 cells/mL with 2.5 mL media in each plate. Cells were allowed 24 hours to attach. After 24 hours, the cells were washed with PBS and pretreatment of either media only, DAC in media (50 ng/mL), or DAC-nanogel in media (50 ng/mL). The samples were left in the incubator with the pretreatment for 3 days after which the cells were washed with PBS and normal media was added. Normal media was changed every other day until 5 days post removal of pretreatment. At that time media was removed and replaced with nanoparticles in media (200 µg of PLGA-based nanoparticles in 2 mL of media) loaded with 6-coumarin dye loaded at 50 µg 6-coumarin per 90 mg PLGA as previously described (Peetla et al. 2014). The nanoparticles in media were added to the cells for 2 hours prior to confocal imaging. A lysotracker stain (Lysotracker Red DND-99, Molecular Probes, Invitrogen, catalog number L7528) was added to half the cell samples 30 minutes prior to imaging at a concentration of 75 ng/mL. The other half of the cell samples were treated with a membrane dye (Cell Mask Deep Red Plasma Membrane Stain, Invitrogen, catalog number C10046) five minutes prior to imaging at a concentration of 5 µg/mL. Immediately before imaging, cells were washed twice with PBS to remove excess nanoparticles and dyes and phenol red free media with DAPI was applied for imaging.

3.7.2 Confocal Microscopy

Live cell imaging was performed using a spinning disk confocal microscope (Ultraview Vox, PerkinElmer, Waltham, MA). Images were captured using alternating illumination with lasers for capturing nanoparticle (6-coumarin) signal (green filter, Ex λ 488) and dye signals for the lysotracker (red filter, Ex λ 561) and cell membrane (deep red filter, Ex λ 640). Stacks of images were taken for each sample in the z-plane. Distance between each 'slice' of a stack is 0.50 µm. Images shown from confocal are single slices for clarity. Magnification for all images was 63X. All images were brightened 50% and sharpened 50% for viewing in print. Image enhancements and processing was done using Image-Pro.

3.7.3 Quantification of Nanoparticle Uptake

Quantification of nanoparticle uptake was done using Excel and Image-Pro. For each cell sample, a stack of images was captured encompassing the entire cell monolayer. Cell monolayers were approximately 11 – 12 µm thick. Images ('slices') were taken 0.5 µm apart, therefore a stack of about 20 images was captured for each cell sample. Five slices, 0.50 µm apart, taken from the middle of each stack was analyzed for the nanoparticles uptake quantification. For each slice, the total intensity of green in the image was determined using Image-Pro. Number of cells in the image was counted in Image-Pro, and the average (of the 5 slices) intensity per cell was calculated in Excel for that sample. There was only one replicate per data point (the slices were of the same sample and many of the cells spanned multiple slices) so there are no statistical calculations shown with this data.

CHAPTER IV

RESULTS AND DISCUSSION

4.1 Results

4.1.1 DAC-nanogel Characterization and Loading

All of the aims include the use of DAC-nanogel. The physical characteristics of the synthesized nanogel before and after loading with DAC are shown in **Table 4**.

Formulation	Efficiency of loading (%)	Loading (%)	Mean diameter (nm)	PI	Zeta potential (mV)
Void nanogel	-	-	209.0	0.05	-21.55
DAC-nanogel	80.52	6.1	227.1	0.05	-19.90

Table 4: Physical characterization of nanogel before (void nanogel) and after (DAC-nanogel) DAC loading. The efficiency of loading refers to the percentage of DAC that was encapsulated out of the entire amount of DAC added to the nanogel. The loading is the weight by weight percentage of DAC to total weight (DAC and nanogel). This data represents one synthesized batch of void nanogel and one batch of loaded nanogel. Refer to the explanation in section 4.1.1 for further information on the samples . PI, polydisperity index.

The mean hydrodynamic diameter, polydisperity index (PI), and zeta potential were determined using a particle sizer as described in section 3.3.1. The void nanogel and DAC-nanogel had a mean diameter of 209.0 nm and 227.1 nm, and zeta potentials of -21.55 mV and -19.90 mV, respectively. Both had a PI of 0.05. This PI is consistent with

previous nanogel batches used in published studies and is less than the general guideline of 0.1 to show uniformity of the sample. The efficiency of loading (amount of DAC inside the nanogel versus total DAC added to the nanogel suspension) for the DAC-nanogel was 80.52 %. The loading (percent weight of DAC to the total – DAC plus nanogel - weight) was 6.1 %. The data in **Table 4** represents one batch of synthesized void nanogel and one batch of DAC loaded nanogel. There are the mean diameter, PI, and zeta potential values for three aliquots of the void nanogel included in the values for void nanogel and six aliquots included in these values for DAC-nanogel included in **Table 4.** The efficiency of loading and loading (by mass) values are $n = 1$ since one batch of DAC-nanogel was prepared and put into aliquots. Then, one of those aliquots was used for DAC –nanogel loading determination using HPLC-UV/VIS, See section 4.2 for more information on the data used in **Table 4**.

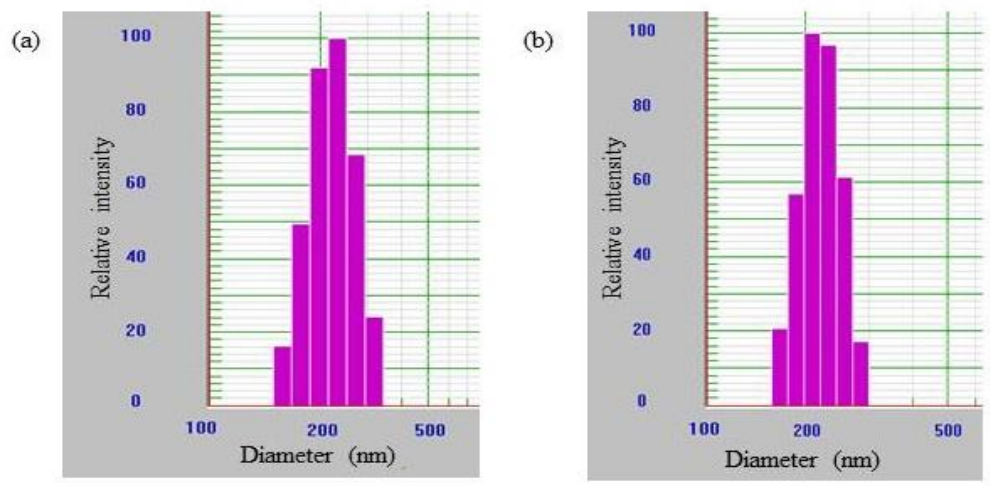

Figure 3: Hydrodynamic diameter and particle size distribution of a void nanogel (a) and DAC-nanogel (b). The mean diameter of the void nanogel shown here is 219.6 nm and the PI is 0.06. The mean diameter of the DAC-nanogel shown here is 223.0 nm and the PI is 0.04.

Representative chromatograms of DAC and DAC-nanogel (after DAC extraction) are shown in **Figure 4.**

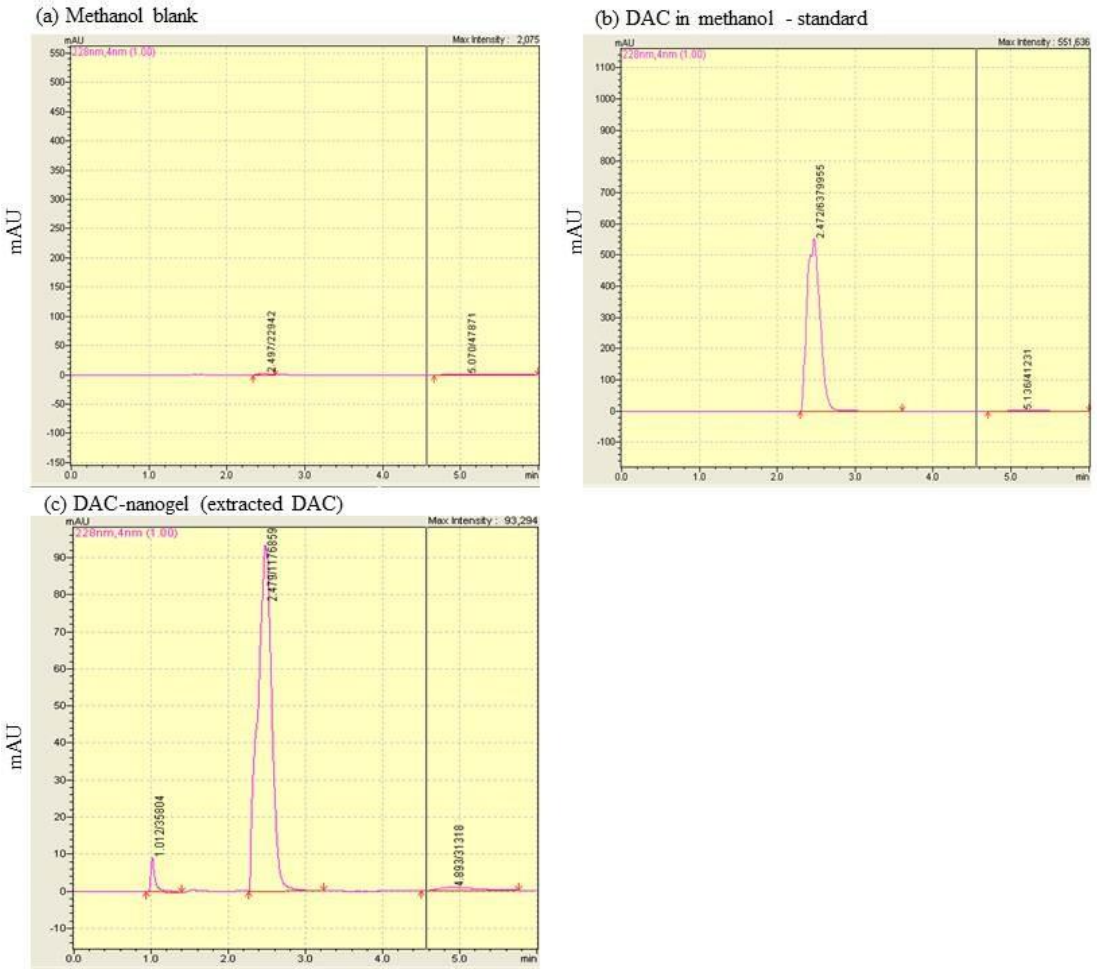

Figure 4: Representative chromatograms from the HPLC-UV/VIS analysis of DAC and DAC-nanogel. Area under the curves is representative of mass. Max intensity listed in the upper right hand corner of each chromatogram as well as the scale on the vertical axis (mAU, milliAbsorbance Units) gives an indication of peak size. (a) Methanol used as blank. Methanol is used for the drug extraction. A small peak of residual DAC can be seen at the approximately 2.5 minute mark. (b) DAC in solution. Note the double peak indicating isomers as discussed below in section 4.2. (c) DAC-nanogel after extraction of the DAC by stirring in methanol overnight and centrifugation.

4.1.2 DAC Stability

The objective of this experiment is to see the stability of DAC Solution (alone) versus DAC-nanogel in mouse plasma (GeneTex Inc. Irvine, CA) at physiological

conditions. The DAC or DAC-nanogel was added to mouse plasma warmed to 37 ºC. Samples were taken at time intervals to observe the stability of the DAC alone versus DAC-nanogel over time.

Figure 5a compares DAC solution with a high concentration (100 µg/mL) to the DAC solution with a low concentration (300 ng/mL) before normalization. The rate constants (K) are 1.069 for the high initial concentration and 1.075 for the low initial concentration. **Figure 5b** compares the same data except it is after normalization so that the first timepoint (t = 0) taken is adjusted to be 100% on the '% DAC remaining' axis on the graph. The rate constants (K) are 1.073 for the high initial concentration and 1.071 for the low initial concentration. The differences in the rate constants (K) are due to differences in rounding during curve calculations in GraphPad Prism between the absolute data and the normalized data. The curves shown are model curves – one phase exponential decay – in all cases.

(a)

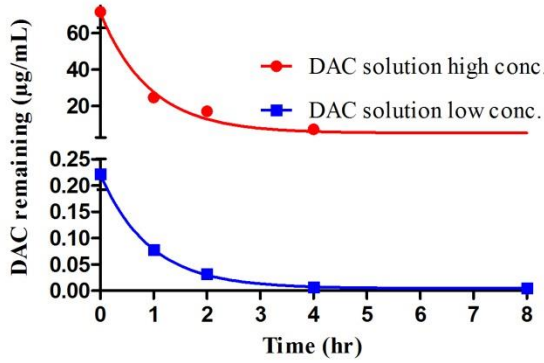

$Y = (Y_0 - Y_{min}) * \exp(-K * t) + Y_{min}$

$Y = (71.20 - 4.981) * \exp(-1.069 * t) + 4.981$

$Y = (0.221 - 0.005) * \exp(-1.075 * t) + 0.005$

	DAC solution high conc.	DAC solution low conc.
Y_0 (µg/mL)	71.20	0.221
Y_{min} (µg/mL)	4.981	0.005
K	1.069	1.075
R square	0.96	0.95
Half Life ($t_{1/2}$) (hr)	0.648	0.645

(b)

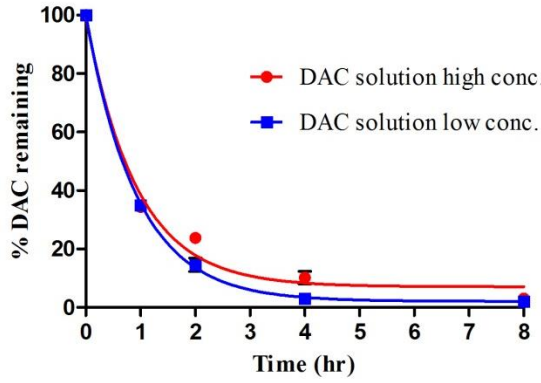

$Y = (Y_0 - Y_{min}) * \exp(-K * t) + Y_{min}$

$Y = (99.25 - 7.135) * \exp(-1.073 * t) + 7.135$

$Y = (99.91 - 2.125) * \exp(-1.071 * t) + 2.125$

	DAC solution high conc.	DAC solution low conc.
Y_0 (%)	99.25	99.91
Y_{min} (%)	7.135	2.125
K	1.073	1.071
R square	0.9868	0.9978
Half Life ($t_{1/2}$) (hr)	0.646	0.647

Figure 5: Stability curves of a high initial DAC concentration (100 µg/mL) (n = 2) in plasma and a relativley low initial DAC concentration (300 ng/mL) (n = 3) in plasma. (a) Absolute concentration values are shown using a segmented y-axis. Error bars designate s.e.m. (b) This data is the same data as in (a) except it is normalized to begin at 100%. Error bars designating s.e.m are included for all points but cannot be seen in (a) and can be seen at only a few points in (b) due to the y-axis constraints and the relatively small values of the s.e.m. data. These high and low concentration curves are combined to form 'DAC solution' in Figure 6.

The data for the two DAC solution curves is combined and normalized to form 'DAC solution' in **Figure 6**. The resulting curves and rate constants (K) are shown and the main focus is that the concentration of DAC in DAC-nanogel is decreasing slower than DAC alone.

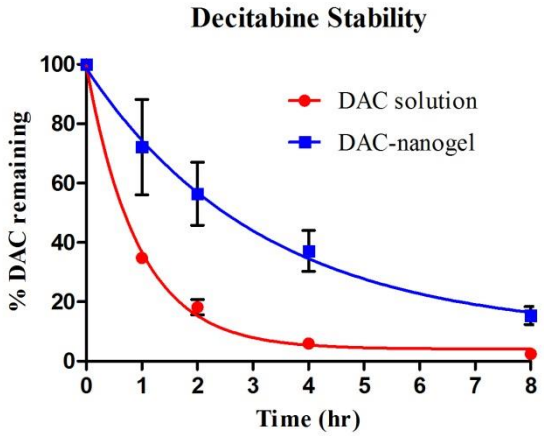

$$Y = (Y_0 - Y_{min}) * \exp(-K * t) + Y_{min}$$

$$Y = (99.64 - 4.128) * \exp(-1.072 * t) + 4.128$$

$$Y = (98.67 - 9.272) * \exp(-0.315 * t) + 9.272$$

	DAC solution	DAC-nanogel
Y_0 (%)	99.64	98.67
Y_{min} (%)	4.128	9.272
K	1.072	0.3154
R square	0.9925	0.7079
Half Life ($t_{1/2}$) (hr)	0.647	2.20

Figure 6: Stability in mouse plasma at physiological conditions. n = 5 for DAC Solution, n = 4 for DAC-nanogel measured using HPLC-MS/MS. Error bars designating s.e.m. are within symbols for certain data points because of the relatively small value of s.e.m. for those points compared to the y-axis . p = 0.033 DAC solution vs. DAC-nanogel.

4.1.3 Duration of Pretreatment

MCF-7/ADR cells were pretreated with DAC solution, DAC-nanogel, or no pretreatment for three or five days. The dose response curve is a measure of their response to subsequent addition of paclitaxel (PTX).

Figures 7 – 9 show that DAC-nanogel pretreatment for a duration of 5 days has an effect on subsequent drug antiproliferative effect significantly greater than the effect of DAC-nanogel pretreatment for a duration of 3 days. The effect occurs at lower concentrations of PTX as shown in **Figure 7**. This could be due to a threshold effect discussed further in section 4.2.

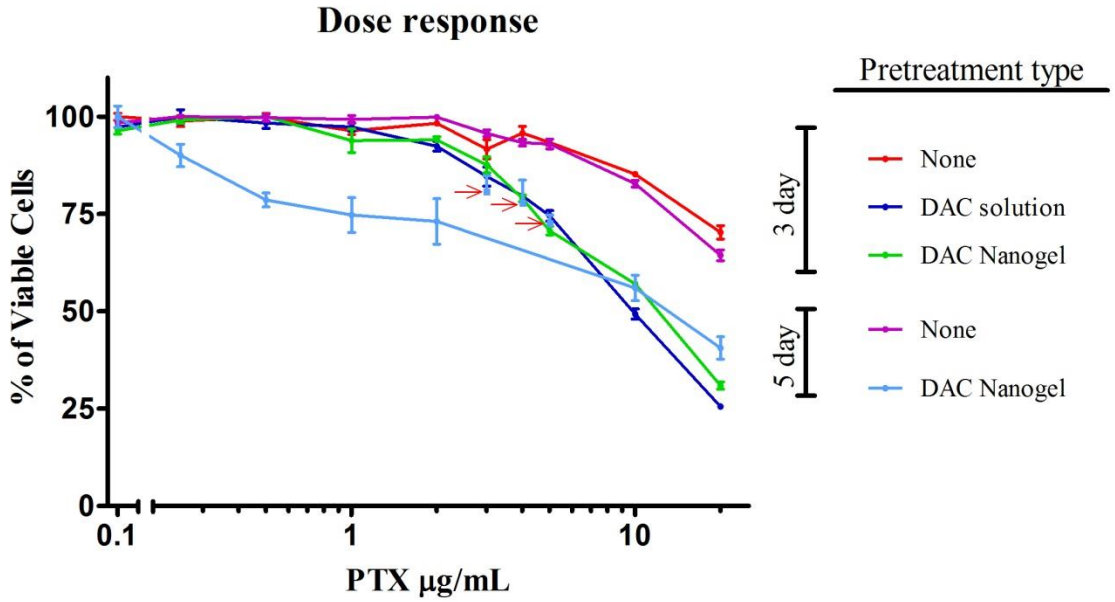

Figure 7: Dose response curves for the different pretreatment types and durations. All samples are normalized with the zero concentration being 100% growth. Three data points in the '5 day DAC Nanogel' group are excluded from the line and IC_{50}/IC_{70} calculations as discussed in the text. n = 6.

Two-way ANOVA statistical analysis was performed to determine whether a duration of 5 days of pretreatment with DAC-nanogel is significantly more effective than a duration of 3 days of pretreatment with DAC-nanogel on the efficacy of PTX as outlined in aim two in section 1.3. The dose response curves are shown separately for 3 day pretreatment and 5 day pretreatment in **Figure 8**.

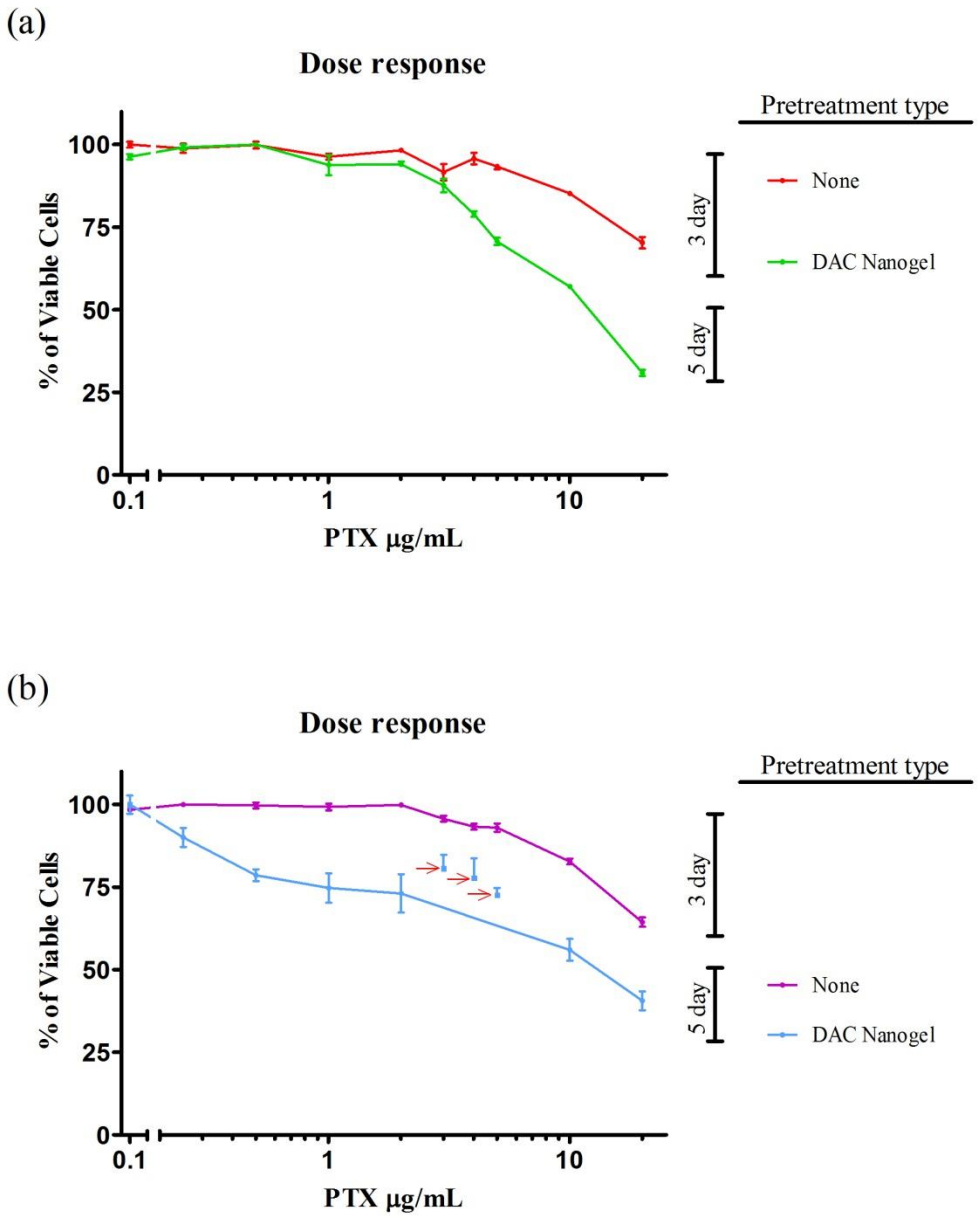

Figure 8: Dose response curves for the different pretreatment types and durations showing (a) 3 day no pretreatment and DAC nanogel pretreatment and (b) 5 day no pretreatment and DAC nanogel pretreatment. All samples are normalized with the zero concentration being 100% growth. Three data points in the '5 day DAC Nanogel' group are excluded from the line and IC_{50}/IC_{70} calculations as discussed in the text. n = 6.

The variable slope lines fit to each set of data to calculate IC_{50} and IC_{70} values are in Appendix A. The IC_{50}/IC_{70} results are shown in **Figure 9**.

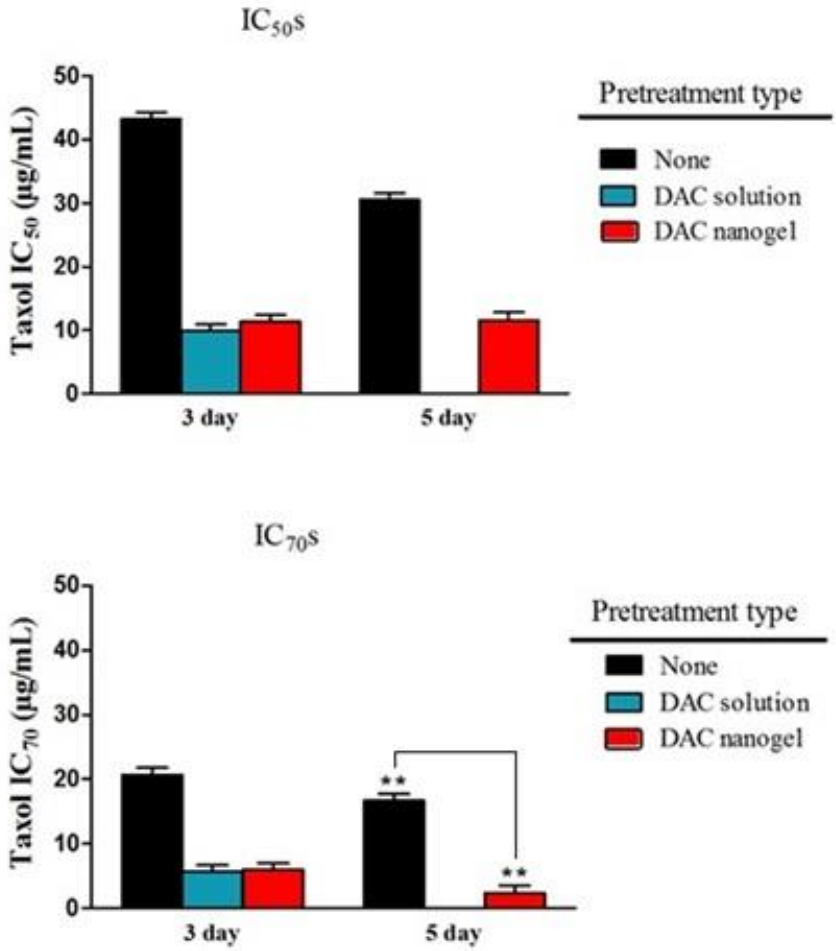

Figure 9: IC_{50} and IC_{70} concentrations. This figure shows the effect of durations of 3 days and 5 days of DAC-nanogel pretreatment on efficacy of subsequent PTX treatment as described in aim two. For the IC_{50}s, the effect of duration on DAC-nanogel pretreatment is not significant. For the IC_{70}s, p = 0.0019 for the significance of the duration of DAC-nanogel pretreatment. The difference in the 'None' pretreatment time is used as a control for the difference in the DAC-nanogel pretreatment type. Further explanation of the two-way ANOVA analysis used to find the significance is described in the text in this section. *n* = 6 for all. Three data points in the '5 day DAC Nanogel' group are excluded from the IC_{50}/IC_{70} calculations as discussed in the text.

The IC_{50} (concentration of the drug which causes 50% of the maximum inhibition of cell viability) for the 3-day incubation with no pretreatment and DAC-nanogel pretreatments are 43.17 ± 1.11 and 11.33 ± 1.03 µg/mL respectively, and 5-day incubation with no pretreatment and DAC-nanogel pretreatments are 30.52 ± 1.04 and

11.61 ± 1.20 µg/mL respectively. The IC_{70}s (concentration of the drug which causes 70% of the maximum inhibition of cell viability) for the 3-day incubation with no pretreatment and DAC-nanogel pretreatments are 20.73 ± 1.06 and 6.01 ± 1.03 µg/mL respectively, and 5-day incubation with no pretreatment and DAC-nanogel pretreatments are 16.68 ± 1.02 and 2.36 ± 1.18 µg/mL, respectively.

The two-way ANOVA analyzes how the IC_{50}/IC_{70} concentrations are influenced by two factors – pretreatment type (none or DAC-nanogel) and duration (3 or 5 days). There is a difference in the 'none' pretreatment type between the 3-day and 5-day for both the IC_{50} and IC_{70} concentrations as can be seen in **Figure 9**. This difference - due to some factor associated with the two day difference in incubation time – affects the antiproliferative effect of the subsequent PTX treatment. This difference (in the no pretreatment group) must serve as a control for the DAC-nanogel pretreatment group. Two-way ANOVA accomplishes this by analyzing whether there is a combination effect of interaction between the duration and the pretreatment type and what the significance of of each of them (duration and pretreatment type) alone is on the results (IC_{50}/IC_{70}). The DAC solution was not used for any statistical analysis since there is not a 5-day sample. Reports from GraphPad Prism with two-way ANOVA results are shown in Appendix B. The two-way ANOVA results concluded that for the IC_{50} data, a difference between the 3-day and 5-day DAC-nanogel cannot be considered significant because of the difference also seen between the 3-day and 5-day no pretreatment samples. The two-way ANOVA results concluded that for the IC_{70} data, a difference between the 3-day and 5-day DAC-nanogel can be considered significant because it is significantly larger than the difference between the 3-day and 5-day no pretreatment samples. This type of comparison is

examining the ratio of a ratio and then determining whether the difference is significant. The significance of the effect of 5-day DAC-nanogel pretreatment (compared to 3-day DAC-nanogel pretreatment) is p = 0.0019. This is the effect of a longer duration with DAC-nanogel which is aim 2 of the research herein.

Note that the DAC solution pretreatment for five days sample was contaminated and is not included in **Figures 7 - 9**. The DAC-nanogel 5 days sample has three data points that indicate an increase in cell proliferation despite increased concentrations of PTX which isn't possibly correct. Those three points are designated by red arrows in the graph but the dose-response curve does not incorporate them and they are not included in IC_{50} or IC_{70} calculations.

4.1.4 Uptake of Nanoparticles

Confocal images in **Figure 10 – Figure 13** show MCF-7/ADR cells with one of three pretreatment types (none, DAC Solution, or DAC Nanogel) and with one of two dyes - Lysotracker, or 'Membrane Stain' (also known as Cell Mask). The Lysotracker appears red in color and stains acidic organelles. The membrane stain appears 'deep red' or purple and stains the plasma membrane. The green color is the nanoparticles loaded with 6-coumarin fluorescent dye. The blue is the cell nuclei dyed with DAPI. Although some cells look larger than others (see **Figure 10** and **Figure 11**), all images are at 63 times magnification. The different size of the nuclei and cells may be due to the degree of confluency in the plate. It can also be seen that the sample with no pretreatment and lysotracker stain looks redder whereas the DAC Solution pretreatment and the DAC Nanogel pretreatment have an orange color. This is due to the amount of green 6-

coumarin nanoparticles that were taken up by the pretreated cells. This can be confirmed by looking at **Figure 12** and noting that when the colors are separated the Lysotracker red looks just as red in all the samples. In **Figure 12**, the Lysotracker stain reveals that the nanoparticles are not trapped in intracellular vesicles such as lysosomes since the green can be seen throughout the cytoplasm and is not just appearing in the same location as the lysotracker stain. In **Figure 13**, although it can be difficult to see the green color in the image, there is some green fluorescence appearing in the No Pretreatment sample. The intent of using a membrane stain was to be able to visualize endocytosis of the nanoparticles by correlating endocytic rate with a decreased signal from the membrane stain (due to stained lipids being endocytosed). In the images in **Figure 13**, the greatest intensity of membrane dye appears in the DAC Nanogel pretreatment group. This could mean that it has the lowest rate of endocytosis (assuming the intensity of membrane stain signal is inversely correlated to nanoparticle uptake) but that would not corroborate the fact that it has the second highest amount of nanoparticle uptake (according to quantified results of 6-coumarin loaded nanoparticle uptake shown in **Figure 14**). The lowest intensity of membrane stain appears to be in the DAC Solution, indicating that it has the highest rate of endocytosis. The highest rate of endocytosis appearing in the DAC solution sample does collaborate with the uptake in nanoparticles being the greatest for this sample as shown in **Figure 14**. The membrane stain did not serve to (inversely) correlate with endocytic rate as evidenced by comparing the signal intensity of the membrane stain in each of the three samples to the quantified uptake results in **Figure 14**. A case for the membrane stain intensity serving as an indicator of endocytic rate could be performed as a proof of concept study as mentioned in section 5.2. The membrane dye

may be useful as a confirmation that the nanoparticles are inside the cells, especially when the images can be seen in 3D, but was not useful in this study. However, the samples that received the membrane dye can still be used for nanoparticle uptake quantification shown in **Figure 14.**

Figure 10: Confocal microscopy images from three pretreatment groups – no pretreatment, DAC (solution), and DAC nanogel. The top row all have been stained with Lysotracker (red). The bottom row have all ben stained with a membrane stain (appearing as a deep red or purple color). All samples have had DAPI added to stain the nuclei blue and 6-coumarin loaded nanoparticles (appearing green). These are single cross sections of one sample for each of the pretreatment groups. All images are 63 times magnified.

Figure 11: These are the same images as those shown in Figure 8 but they are enlarged to show details. Confocal microscopy images from three pretreatment groups – no pretreatment, DAC (solution), and DAC nanogel. The top row all have been stained with Lysotracker (red). The bottom row have all ben stained with a membrane stain (appearing as a deep red or purple color). All samples have had DAPI added to stain the nuclei blue and 6-coumarin loaded nanoparticles (appearing green). These are single cross sections of one sample for each of the pretreatment groups. All images are 63 times magnified.

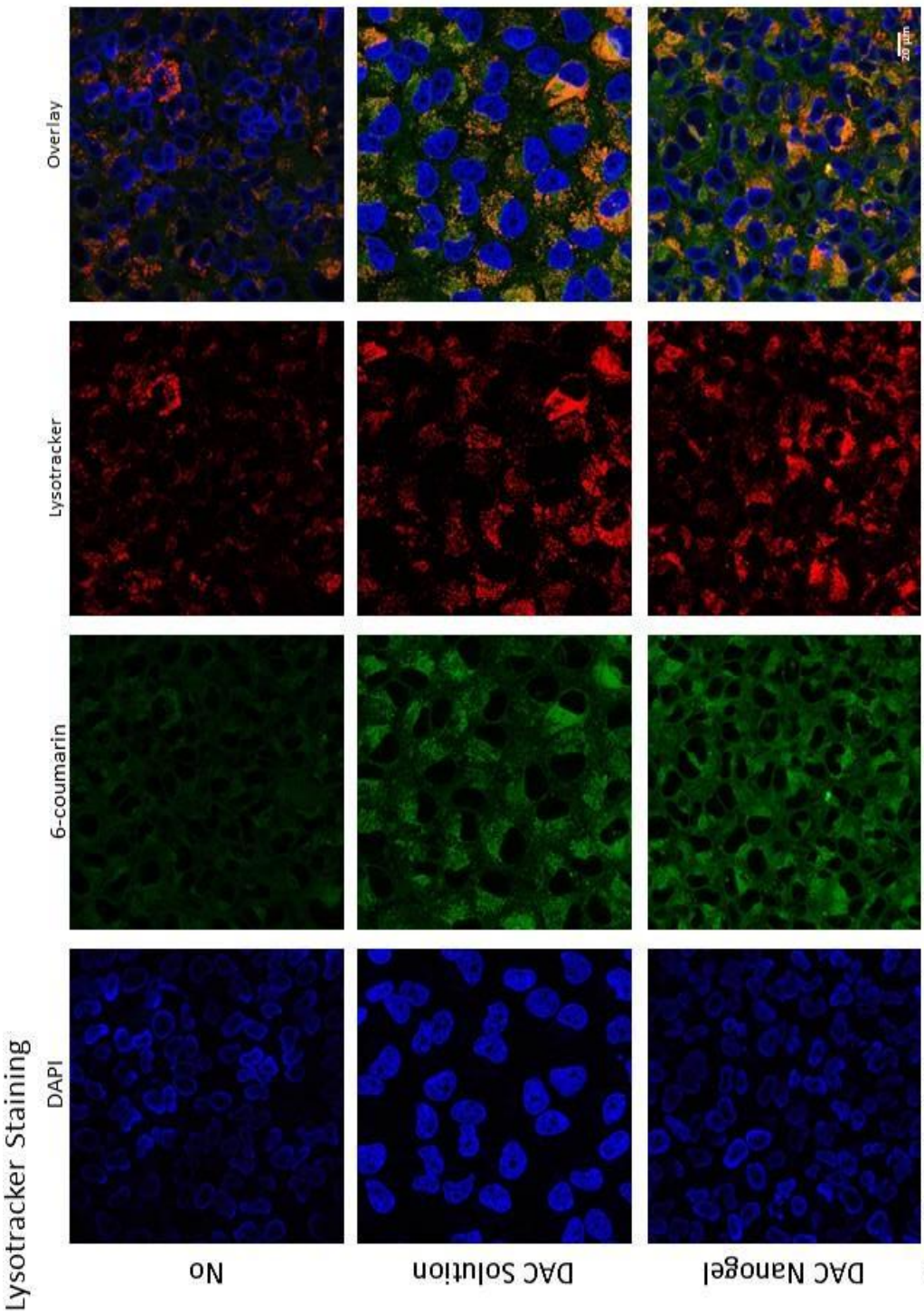

Figure 12: Confocal microscopy images from three pretreatment groups – no pretreatment (top row), DAC (solution) (middle row), and DAC nanogel (bottom row). The first column shows the DAPI (blue) stained nuclei. The second column shows the 6-coumarin (green) nanoparticles. The third column shows the lysotracker (red) stained lysosomes. The fourth column is an overlay image of the first three columns combined. These are single cross sections of one sample for each of the pretreatment groups. All images are 63 times magnified.

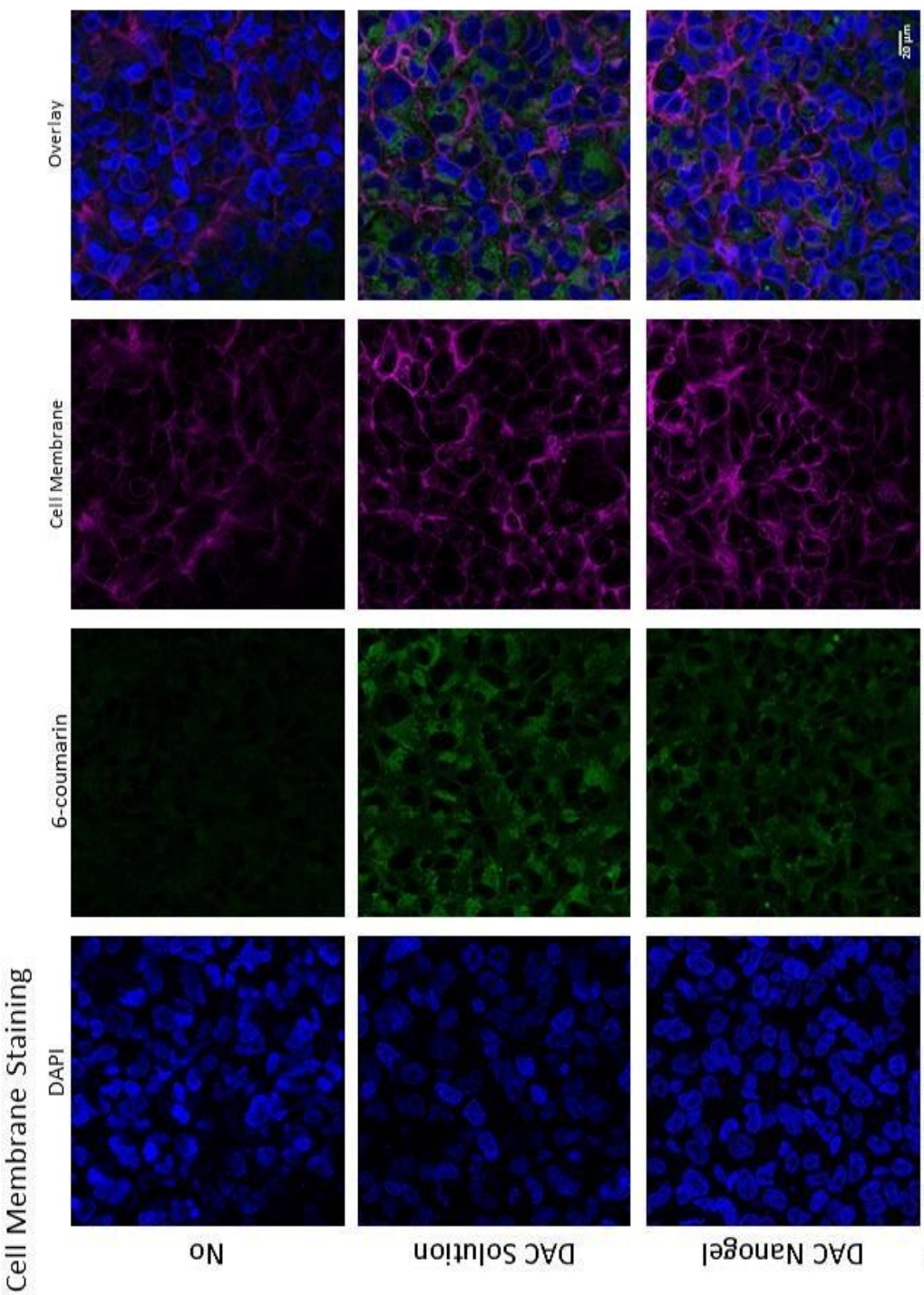

Figure 13: Confocal microscopy images from three pretreatment groups – no pretreatment (top row), DAC (solution) (middle row), and DAC nanogel (bottom row). The first column shows the DAPI (blue) stained nuclei. The second column shows the 6-coumarin (green) nanoparticles. The third column shows the Cell Membrane (deep red or purple) stained lipid membranes. The fourth column is an overlay image of the first three columns combined. These are single cross sections of one sample for each of the pretreatment groups. All images are 63 times magnified.

The intensity of the green fluorescence was quantified for each sample (no pretreatment, DAC solution pretreatment, and DAC nanogel pretreatment) from the confocal images is shown in **Figure 14**.

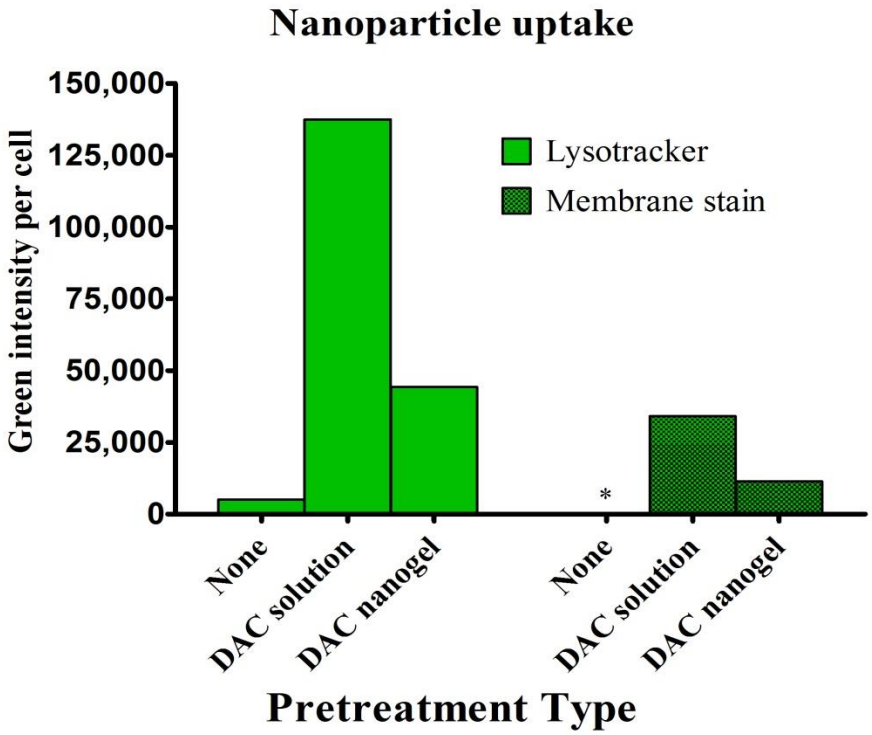

Figure 14: Quantification of nanoparticles loaded with 6-coumarin (green) intensity in MCF-7/ADR cells. Each bar represents one sample, n = 1 (although the total green intensity of each image was divided by the number of cells in that image, the green intensity inside any individual cell was not determined for this study). * Note that the bar for the Membrane stain - no pretreatment sample is not zero, it is 81.

The total intensity of the green (indicating nanoparticles) in each image was divided by the number of cells in that image to account for the different numbers of cells between images. For both stains, the graph shows that the DAC solution pretreatment caused the greatest increase in nanoparticle uptake and the DAC nanogel pretreatment caused an increase as well, although not as large. For the Lysotracker stain group, the DAC solution increases uptake by 27 times, and DAC nanogel increases uptake 9 times over the

control. In the cell membrane stain group, the DAC solution increases uptake by 421 times, and DAC nanogel increases uptake 141 times over the control. The reason for the discrepancy in green fluorescence / nanoparticle uptake between the two dyes is not clear. Since the overall uptake is lower in the cells treated with the cell membrane stain, it could be that the stain is interfering with endocytosis of the nanoparticles. It is not the case that the membrane stain color is interfering with the resulting green intensity. The confocal microscopy prevents this from happening by capturing the different colors independently and consecutively (not all in one image at one time).

4.2 Discussion

The physical characterization of the nanogel before and after DAC loading is comparable to previous research performed by Vijayaraghavalu and Labhasetwar (2013) from which the method of nanogel synthesis, loading, and loading determination was adapted. The loading (and loading efficiency) was within the s.e.m. of the previous research (the DAC-nanogel loading and loading efficiency from the previous research was 80 ± 5 % and 6.4 ± 0.4 %, respectively, and 80.52 % and 6.1 %, respectively for this study herein). The loading of the nanogel was determined using HPLC-UV/VIS according to the method in previous research by Vijayaraghavalu and Labhasetwar (2013). The chromatograms shown in **Figure 4** show that DAC can have a double peak which is not entirely separated but there are two apexes. This was confirmed by mass spectrometry during the DAC in plasma stability study to be two isomers of DAC. Therefore, total area under both peaks is included for the DAC analysis.

The mean diameter, PI, and zeta potential values are determined to assess continuity between batches so that experimental results can be considered comparable. Mean diameter of the void nanogel and DAC-nanogel was larger in this study (the void nanogel and DAC-nanogel mean diameter from the previous research was 233 nm and 244 nm, respectively, and 209.0 nm and 227.1 nm, respectively for this study herein). It is unknown whether the difference in mean diameter is significant since there is not a value given for the s.e.m. for the previous research.

Polydisperity index (PI) was lower in this study (the void nanogel and DAC-nanogel PI from the previous research was 0.06 and 0.11, respectively, and 0.05 and 0.05, respectively for this study herein). The sonication step was optimized for this study to achieve a low PI and not create foam as outlined in section 3.3.2. A PI less than 0.1 - which was the case for all samples in this study - is a general guideline that indicates uniformity of the sample. Particle size distribution around the mean diameter can be observed by the distribution graph from the dynamic light scattering as shown in **Figure 3**. The distribution of the nanogels is similar to the distribution shown in the previous research by Vijayaraghavalu and Labhasetwar (2013), as would be predicted based on the values for the mean diameter and the polydisperity index also being similar. The PI also serves as a confirmation that the sonication has successfully dispersed the nanogel.

The zeta potential was within the s.e.m. from the previous research (the void nanogel and DAC-nanogel zeta potential from the previous research was -25 ± 4.0 mV and -19 ± 1.0 mV, respectively, and -21.55 mV and -19.90 mV, respectively for this study herein). The zeta potential is related to the electrical surface potential of the

nanogel (but not the same as particle charge). It is a measure of the electrical potential difference at the location of the slipping plane and is a key indicator of stability of a colloidal dispersion. It was used in this study as another means of comparison of the current nanogel with previous research to assess whether the different nanogel batches are comparable. The results from the DAC stability analysis verify that increased stability of DAC in nanogel could be a reason for the greater efficacy seen when using DAC-nanogel rather than DAC solution in previous studies (Vijayaraghavalu and Labhasetwar 2013; Raghavan et al. 2015). A high and a low concentration of DAC solution provide a range within which to compare the stability curve to DAC-nanogel as suggested in the American Association of Pharmaceutical Scientists Journal (van de Merbel et al. 2014). A concentration of 50 ng/mL DAC (the concentration used as pretreatment in the IC_{50}/IC_{70} and confocal experiments) as the beginning concentration would not have produced a detectable stability curve because the lower limit of quantification (LLOQ) for the HPLC - mass spectrometry method was 40 ng/mL DAC. The concentration of 100 µg/mL was chosen while optimizing the protocol to be high enough that a stability curve could be observed. Patient data showing 300 ng/mL (1 µM DAC is equal to 228 ng/mL) to be a clinically relevant concentration (Karahoca and Momparler 2013). The DAC-nanogel did not reach a plateau during the experiment. This is reflected in the value of Y_{min} which is extrapolated out and found to be 9.27, which is past the time of the last sample taken at 8 hours. The absolute values or kinetics from this stability study are not relevant *in vivo* as there are many more factors in play in animal models/clinical studies such as renal clearance and drug metabolism. But as a mechanistic and comparative study it is useful in developing new theories and experiments that could lead to *in vivo* or

clinical studies. The increased stability of the DAC in nanogel (half- lives of the DAC and the DAC in nanogel were 39 minutes and 2 hours 12 minutes, respectively) also provides a mechanism by which a longer duration of the DAC-nanogel pretreatment is leading to greater efficacy of the subsequent anticancer drug as shown in the IC_{50} and IC_{70} values in **Figure 9.**

The dose response curves and IC_{70} values correlate with the stability data by supporting the hypothesis that DAC is more stable in nanogel by showing that the DAC-nanogel 5-day pretreatment has the greatest effect on subsequent drug efficacy. However, the effect is not seen at high concentrations of PTX. This could be because at these very high concentrations, enough PTX is intracellular that the efficacy is the same for the pretreated samples. It has been shown in a previous study that this can be the case where there is a threshold affect (Peetla et al. 2010). Doxorubicin is a preferred drug for treating breast cancer but PTX is rather a broader spectrum anticancer drug used for treating different types of cancers.

The confocal experiment showed that the greatest increase in nanoparticle uptake occurred in the DAC solution pretreated cells, not DAC-nanogel pretreated as was hypothesized. It could be that if more time had elapsed since pretreatment with DAC then the DAC-nanogel would have had the greater effect on uptake. The protocol for the confocal experiment requires 3 days of incubation with pretreatment, then the confocal and nanoparticle addition is performed 5 days after the removal of the pretreatment. One study in particular has shown that timing of the experiment could impact whether the DAC solution of DAC-nanogel seem to be having a greater impact (Vijayaraghavalu and Labhasetwar 2013). In that study, DAC solution has a more pronounced affect at an

earlier timepoint with regards to antiproliferative effect (of the DAC/DAC-nanogel itself), DNMT1 depletion, and cell cycle arrest. But then at later timepoints in all these aspects, the sustained effect of DAC-nanogel reverses the earlier trend in drug resistant cells. Although in that study, the measured responses are not nanoparticle uptake or perhaps membrane lipid alterations, the sustained effect that DAC-nanogel confers may be applicable to understanding the DAC solution efficacy at one timepoint for the confocal data. There are not any timepoints from that previous study that exactly match the pretreatment duration and post-treatment time of the confocal experiment for a more direct comparison. Previous study showing that DAC-nanogel caused a greater decrease in cholesterol-SM rafts than DAC solution and this phenomenon increased from one day post DAC or DAC-nanogel treatment to 5 days and 8 days post treatment (Raghavan et al. 2015). Since the rafts confer greater rigidity, DAC-nanogel pretreatment would increase fluidity and thereby should have a greater uptake of nanoparticles than the solution treated group. Accordingly, the nanoparticle uptake should have been greater in DAC-nanogel treated cells than in DAC solution treated cells. However, in the previous study where lipid changes were analyzed, the medium was changed and hence DAC remained in the culture medium whereas for confocal microscopy study the medium was replaced after 3 days. Even though the DAC solution had a greater effect, the DAC-nanogel effect was still 9 and 141 – fold higher (for lysotracker and membrane stain, respectively) than the control and DAC-nanogel confers benefits over DAC solution *in vivo* as outlined previously.

CHAPTER V

CONCLUSIONS AND RECOMMENDATIONS

5.1 Conclusions

All experiments proved some benefit of DAC and/or DAC-nanogel pretreatment to overcome drug resistance. The stability of DAC in nanogel was proven to be greater than DAC alone (the half-lives were 2 hours 12 minutes and 39 minutes, respectively) in mouse plasma under physiological conditions using HPLC/MS. The effect of different durations of pretreatment on subsequent anticancer drug efficacy in MCF-7/ADR cells was found using MTS assays. The results show that DAC-nanogel pretreatment for a duration of 5-days causes the greatest increase in efficacy. At the higher doses all pretreatments have a similar response. This is why both IC_{50} and IC_{70} were calculated for further comparison of the data. IC_{50}s of pretreated cells were lower than cells without pretreatment, but there was no significant difference between DAC solution and DAC-nanogel at 3 days. IC_{70} showed a significant difference for the DAC-nanogel 5-day pretreatment sample compared to the DAC-nanogel 3-day sample and accounting for the difference seen in the control (no pretreatment) sample. The effect of DAC and DAC-

nanogel pretreatment on the subsequent uptake of nanoparticles in drug resistant breast cancer cells was visualized using confocal microscopy and the uptake of nanoparticles was quantified using the green intensity per cell. At 5 days following a 3-day pretreatment, the confocal data showed that DAC solution had the greatest increase in uptake of nanoparticles (27 and 421 fold increases with respect to untreated cells) followed by DAC-nanogel (9 and 141 fold increases with respect to untreated cells). The images showed that nanoparticles are not trapped in intracellular vesicles based on the green nanoparticles being seen throughout the cytoplasm, not preferentially overlapping with the red lysosome stain.

5.2 Recommendations

1. There are benefits of nanogel that have been postulated but have yet to be verified. For instance, nanogel may protect DAC from cytidine deaminase in the liver and/or decreases bone marrow toxicity by causing less DAC to pass into the bone marrow.

2. It would be interesting to see what the stability of DAC versus DAC-nanogel looks like when carried out in liver tissue (instead of plasma) under physiological conditions.

3. The polyethylene glycol (PEG) on the nanogel surface should cause an increase in circulation time and cause more accumulation at the tumor site passively via the enhanced permeability (EPR) effect. This hypothesis could be tested.

4. Nanogel surfaces could be made with actively targeting ligands for increased tumor accumulation.

5. Perform a proof of concept study for corroborating deep red plasma stain (membrane dye) with endocytotic rate using cells with varying known endocytotic rates.

6. DAC crosses the membrane via human equilibrative nucleoside transporter 1 (hENT1). It has been proposed that the increased efficacy of DAC-nanogel could be due to the nanogel crossing the membrane via an endocytic mechanism instead of hENT1. This different mode of membrane transportation could affect the conversion rate of intracellular DAC into its active form - DAC-triphospate – which is incorporated into the DNA (Vijayaraghavalu and Labhasetwar 2013). Whether or not DAC-nanogel enters the cell via hENT1 could be studied using a hENT1 specific inhibitor such as S-(4-nitrobenzyl)-6-thioinosine (NBTI) on cells. These hENT1 deficient cells could then be treated with DAC-nanogel. The amount of intracellular DAC in these hENT1 deficient cells could then be directly quantified using a HPLC-MS/MS method such as the one described in this paper. If hENT1 inhibition does not cause a change in intracellular DAC this would indicate that DAC-nanogel crosses the membrane differently than DAC and vice versa.

7. A HPLC-MS/MS method for quantifying intracellular DAC-triphosphate has been developed and validated (Wang et al. 2013). This could be used to determine if the conversion rate of DAC to its active form – DAC-triphosphate – differs between DAC-nanogel and DAC treatment.

8. The confocal data quantifying the uptake of nanoparticles is n = 1. The same experiment could be carried out but with more replicates (n = 3 or greater).

REFERENCES

1. Bird, A. (2007). Perceptions of epigenetics. *Nature*, *447*(7143), 396-398.

2. Issa, J. P. J. (2011). Epigenetics in cancer: what's the future?. *Oncology*,*25*(3), 220.

3. Brown, R., & Plumb, J. A. (2004). Demethylation of DNA by decitabine in cancer chemotherapy. *Expert Review of Anticancer Therapy*, *4*(4), 501-510.

4. Brünner, N., Bronzert, D., Vindeløv, L. L., Rygaard, K., Spang-Thomsen, M., & Lippman, M. E. (1989). Effect on growth and cell cycle kinetics of estradiol and tamoxifen on MCF-7 human breast cancer cells grown in vitro and in nude mice. *Cancer Research*, *49*(6), 1515-1520.

5. Cramer, S. A., Adjei, I. M., & Labhasetwar, V. (2015). Advancements in the delivery of epigenetic drugs. *Expert Opinion on Drug Delivery*, *12*(9), 1501-1512.

6. Damaraju, V. L., Mowles, D., Yao, S., Ng, A., Young, J. D., Cass, C. E., & Tong, Z. (2012). Role of human nucleoside transporters in the uptake and cytotoxicity of azacitidine and decitabine. *Nucleosides, Nucleotides and Nucleic Acids*, *31*(3), 236-255.

7. Demircan, B., Dyer, L. M., Gerace, M., Lobenhofer, E. K., Robertson, K. D., & Brown, K. D. (2009). Comparative epigenomics of human and mouse mammary tumors. *Genes, Chromosomes and Cancer*, *48*(1), 83-97.

8. Escribá, Pablo V., José M. González-Ros, Félix M. Goñi, Paavo KJ Kinnunen, Lászlo Vigh, Lissete Sánchez-Magraner, Asia M. Fernández, Xavier Busquets, Ibolya Horváth, and Gwendolyn Barceló-Coblijn (2008). Membranes: a meeting point for lipids, proteins and therapies. *Journal of Cellular and Molecular Medicine*, *12*(3), 829-875.

9. Esteller, M. (2007). Cancer epigenomics: DNA methylomes and histone-modification maps. *Nature Reviews Genetics*, *8*(4), 286-298.

10. Fvasconcellos. Decitabine.svg. Created 3 October 2007 (UTC). Retrieved on May 11, 2016 from https://commons.wikimedia.org/wiki/File:Decitabine.svg.

11. Goldberg, A. D., Allis, C. D., & Bernstein, E. (2007). Epigenetics: a landscape takes shape. *Cell*, *128*(4), 635-638.

12. Gopisetty, G., Ramachandran, K., & Singal, R. (2006). DNA methylation and apoptosis. *Molecular Immunology*, *43*(11), 1729-1740.

13. Gottesman, M. M. (2002). Mechanisms of cancer drug resistance. *Annual review of medicine*, *53*(1), 615-627.

14. Hendrich, A. B., & Michalak, K. (2003). Lipids as a target for drugs modulating multidrug resistance of cancer cells. *Current Drug Targets*, *4*(1), 23-30.

15. Hollenbach, P. W., Nguyen, A. N., Brady, H., Williams, M., Ning, Y., Richard, N., ... & MacBeth, K. J. (2010). A comparison of azacitidine and decitabine activities in acute myeloid leukemia cell lines. *PloS one*, *5*(2), e9001.

16. Jabbour, E., Issa, J. P., Garcia-Manero, G., & Kantarjian, H. (2008). Evolution of decitabine development. *Cancer*, *112*(11), 2341-2351.

17. Jones, P. A. (2012). Functions of DNA methylation: islands, start sites, gene bodies and beyond. *Nature Reviews Genetics*, *13*(7), 484-492.

18. Jones, P. A., & Takai, D. (2001). The role of DNA methylation in mammalian epigenetics. *Science*, *293*(5532), 1068-1070.

19. Jordheim, L. P., Durantel, D., Zoulim, F., & Dumontet, C. (2013). Advances in the development of nucleoside and nucleotide analogues for cancer and viral diseases. *Nature Reviews Drug Discovery*, *12*(6), 447-464.

20. Kabanov, A. V., & Vinogradov, S. V. (2009). Nanogels as pharmaceutical carriers: finite networks of infinite capabilities. *Angewandte Chemie International Edition*, 48(30), 5418-5429.

21. Karahoca, M., & Momparler, R. L. (2013). Pharmacokinetic and pharmacodynamic analysis of 5-aza-2'-deoxycytidine (decitabine) in the design of its dose-schedule for cancer therapy. *Clinical Epigenetics*, *5*(1), 1.

22. Knappskog, S., & Lønning, P. E. (2012). P53 and its molecular basis to chemoresistance in breast cancer. *Expert Opinion on Therapeutic Targets*,*16*(sup1), S23-S30.

23. Momparler, R. L., Bouffard, D. Y., Momparler, L. F., Dionne, J., Bélanger, K., & Ayoub, J. (1997). Pilot phase l-ll study on 5-aza-2'-deoxycytidine (Decitabine) in patients with metastatic lung cancer. *Anti-cancer Drugs*, *8*(4), 358-368.

24. Nakao, M. (2001). Epigenetics: interaction of DNA methylation and chromatin. *Gene*, *278*(1), 25-31.

25. Neupane, Y. R., Srivastava, M., Gyenwalee, S., Ahmad, N., Soni, K., & Kohli, K. (2015). Solid Lipid Nanoparticles for Oral Delivery of Decitabine: Formulation Optimization, Characterization, Stability and Ex-Vivo Gut Permeation Studies. *Science of Advanced Materials*, 7(3), 433-445.

26. Oloumi, A., Maidan, M., Lock, F. E., Tearle, H., McKinney, S., Muller, W. J., ... & Dedhar, S. (2010). Cooperative signaling between Wnt1 and integrin-linked

kinase induces accelerated breast tumor development. *Breast Cancer Research*, *12*(3), R38.

25. Onda, K., Suzuki, R., Tanaka, S., Oga, H., Oka, K., & Hirano, T. (2012). Decitabine, a DNA methyltransferase inhibitor, reduces P-glycoprotein mRNA and protein expressions and increases drug sensitivity in drug-resistant MOLT4 and Jurkat cell lines. *Anticancer Research*, *32*(10), 4439-4444.

27. Pallarés-Trujillo, J. A. V. I. E. R., López-Soriano, F. J., & Argilés, J. M. (2000). Lipids: A key role in multidrug resistance?(Review). *International Journal of Oncology*, *16*(4), 783-881.

28. Peetla, C., Bhave, R., Vijayaraghavalu, S., Stine, A., Kooijman, E., & Labhasetwar, V. (2010). Drug resistance in breast cancer cells: biophysical characterization of and doxorubicin interactions with membrane lipids. *Molecular Pharmaceutics*, *7*(6), 2334-2348.

29. Peetla, C., Jin, S., Weimer, J., Elegbede, A., & Labhasetwar, V. (2014). Biomechanics and thermodynamics of nanoparticle interactions with plasma and endosomal membrane lipids in cellular uptake and endosomal escape. *Langmuir*, *30*(25), 7522-7532.

30. Peetla, C., Vijayaraghavalu, S., & Labhasetwar, V. (2013). Biophysics of cell membrane lipids in cancer drug resistance: implications for drug transport and drug delivery with nanoparticles. *Advanced Drug Delivery Reviews*, *65*(13), 1686-1698.

31. Perez-Tomas, R. (2006). Multidrug resistance: retrospect and prospects in anti-cancer drug treatment. *Current Medicinal Chemistry*, *13*(16), 1859-1876.

32. Raghavan, V., Vijayaraghavalu, S., Peetla, C., Yamada, M., Morisada, M., & Labhasetwar, V. (2015). Sustained Epigenetic Drug Delivery Depletes Cholesterol–Sphingomyelin Rafts from Resistant Breast Cancer Cells, Influencing Biophysical Characteristics of Membrane Lipids. *Langmuir*, *31*(42), 11564-11573.

33. Rogstad, D. K., Herring, J. L., Theruvathu, J. A., Burdzy, A., Perry, C. C., Neidigh, J. W., & Sowers, L. C. (2009). Chemical decomposition of 5-aza-2′-deoxycytidine (Decitabine): kinetic analyses and identification of products by NMR, HPLC, and mass spectrometry. *Chemical Research in Toxicology*, 22(6), 1194-1204.

34. Santini, V., Kantarjian, H. M., & Issa, J. P. (2001). Changes in DNA methylation in neoplasia: pathophysiology and therapeutic implications. *Annals of Internal Medicine*, *134*(7), 573-586.

35. Slotte, J. P., & Bierman, E. L. (1988). Depletion of plasma-membrane sphingomyelin rapidly alters the distribution of cholesterol between plasma membranes and intracellular cholesterol pools in cultured fibroblasts. *Biochemical Journal*, *250*(3), 653-658.

36. Solyanik, G. I. (2010). Multifactorial nature of tumor drug resistance. *Experimental Oncology*, *32*(3), 181-5.

37. Stresemann, C., & Lyko, F. (2008). Modes of action of the DNA methyltransferase inhibitors azacytidine and decitabine. *International Journal of Cancer*, *123*(1), 8-13.

38. Szakács, G., Paterson, J. K., Ludwig, J. A., Booth-Genthe, C., & Gottesman, M. M. (2006). Targeting multidrug resistance in cancer. *Nature Reviews Drug Discovery*, *5*(3), 219-234.

39. van de Merbel, Nico, Natasha Savoie, Manish Yadav, Yoshiaki Ohtsu, Joleen White, Maria Francesca Riccio, Kelly Dong, Ronald de Vries, and Julie Diancin. (2014). Stability: recommendation for best practices and harmonization from the Global Bioanalysis Consortium Harmonization Team. *The AAPS Journal*, *16*(3), 392-399.

40. Vijayaraghavalu, S., & Labhasetwar, V. (2013). Efficacy of decitabine-loaded nanogels in overcoming cancer drug resistance is mediated via sustained DNA methyltransferase 1 (DNMT1) depletion. *Cancer Letters*, *331*(1), 122-129.

41. Vijayaraghavalu, S., Peetla, C., Lu, S., & Labhasetwar, V. (2012). Epigenetic modulation of the biophysical properties of drug-resistant cell lipids to restore drug transport and endocytic functions. *Molecular Pharmaceutics*, *9*(9), 2730-2742.

42. Wang, H., Chen, P., Wang, J., Santhanam, R., Aimiuwu, J., Saradhi, U.V., Liu, Z., Schwind, S., Mims, A., Byrd, J.C. and Grever, M.R. (2013). In vivo quantification of active decitabine-triphosphate metabolite: a novel pharmacoanalytical endpoint for optimization of hypomethylating therapy in acute myeloid leukemia. *The AAPS Journal*, *15*(1), 242-249.

43. Xu, H., Qiao, M., Fu, Y., Jiang, X., Jin, Y., Li, C., & Yuan, B. (2012). Development and validation of a liquid chromatography–tandem mass spectrometry method for

quantification of decitabine in rat plasma. *Journal of Chromatography B, 899*, 81-85.

44. Yang, X., Lay, F., Han, H., & Jones, P. A. (2010). Targeting DNA methylation for epigenetic therapy. *Trends in Pharmacological Sciences*, *31*(11), 536-546.

APPENDIX A

Nonlinear fit curves for IC_{50} and IC_{70} calculations from *section 4.1.3*.

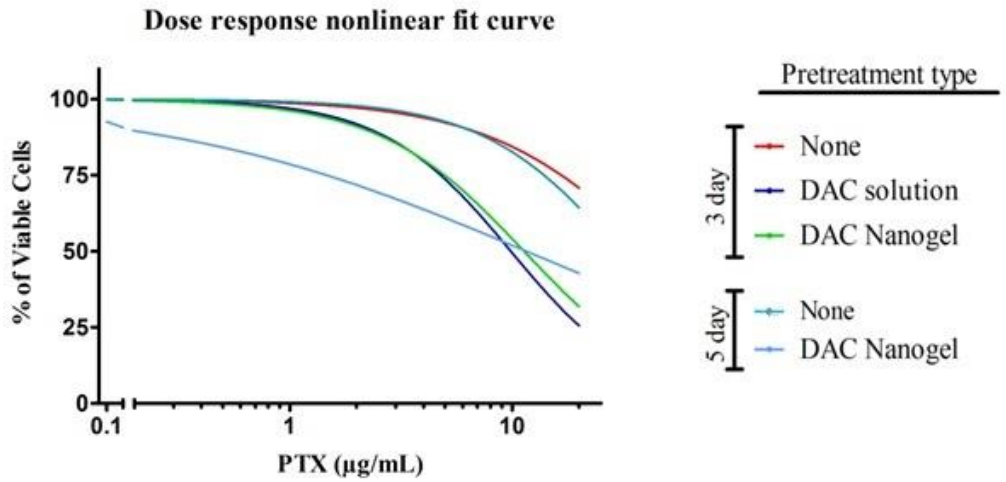

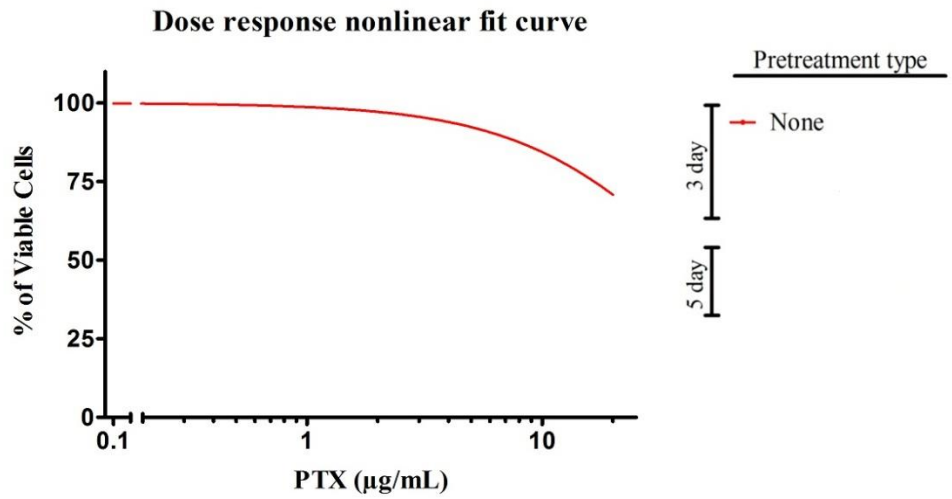

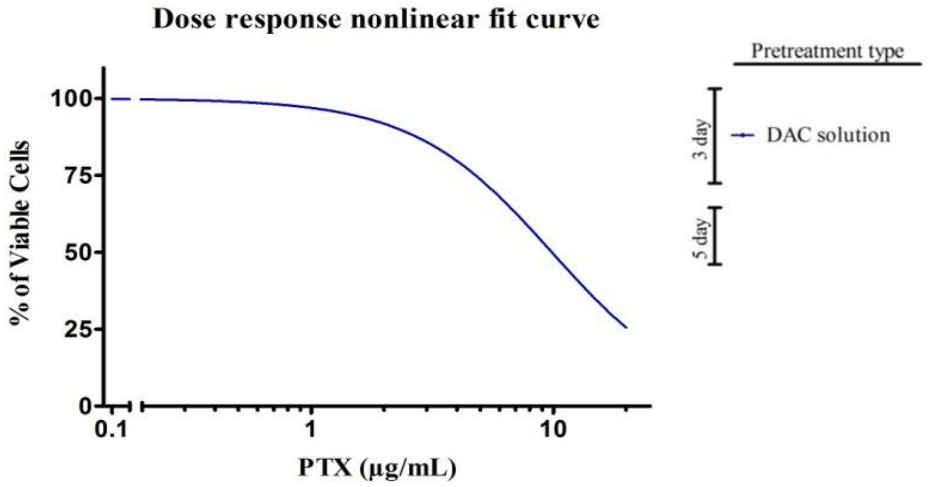

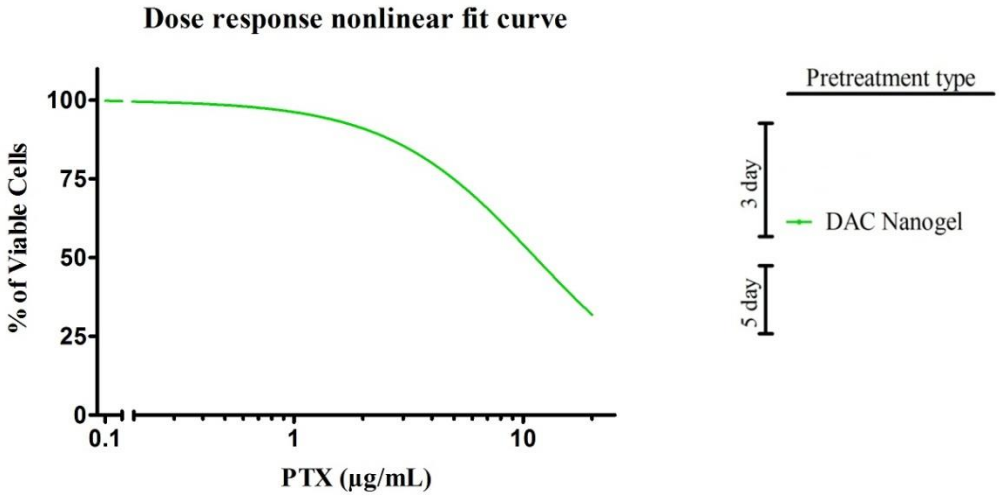

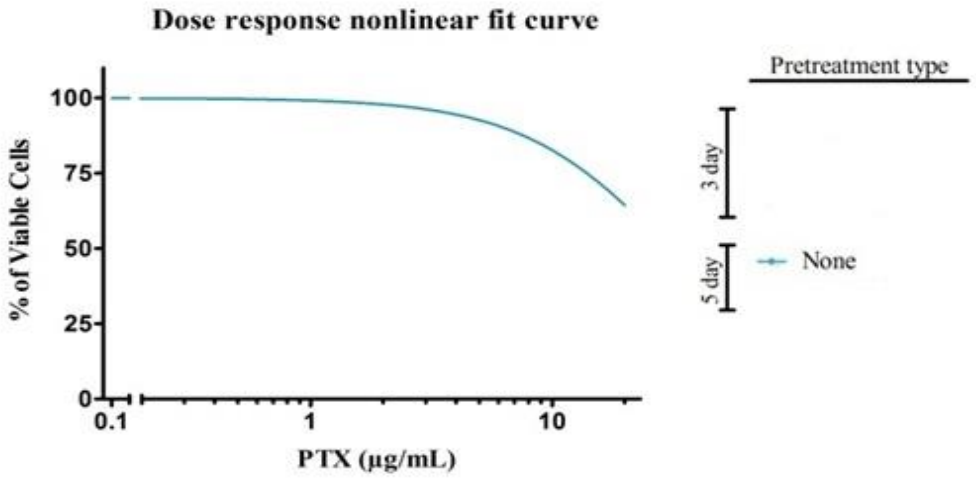

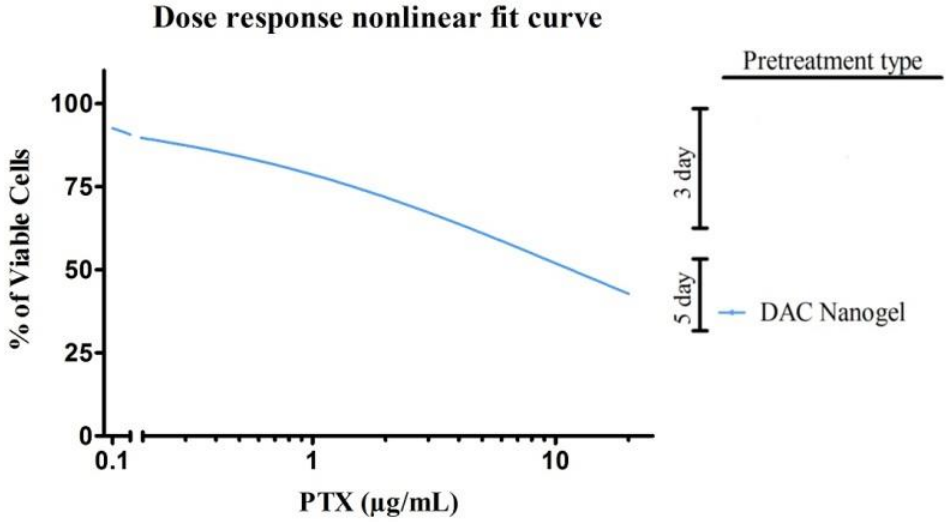

APPENDIX B

Two-way ANOVA results from GraphPad Prism.

Data analyzed: IC50s

Source of Variation	Degrees of Freedom	Sum of Squares	Mean square
Duration	1.0	229.6	229.6
Pretreatment	1.0	3864	3864
Interaction	1.0	251.3	251.3
Residual (error)	20.0	144.9	7.245
Total	23.0	4489	

Does Duration have the same effect at all values of Pretreatment?

Interaction accounts for 5.60% of the total variance.
F = 34.68. DFn=1 DFd=20
The P value is < 0.0001
If there is no interaction overall, there is a less than 0.01% chance of randomly observing so much interaction in an experiment of this size. The interaction is considered extremely significant.

Since the interaction is statistically significant, the P values that follow for the row and column effects are difficult to interpret.

Does Duration affect the result?

Duration accounts for 5.11% of the total variance.
F = 31.69. DFn=1 DFd=20
The P value is < 0.0001
If Duration has no effect overall, there is a less than 0.01% chance of randomly observing an effect this big (or bigger) in an experiment of this size. The effect is considered extremely significant.

Does Pretreatment affect the result?

Pretreatment accounts for 86.06% of the total variance.
F = 533.27. DFn=1 DFd=20
The P value is < 0.0001
If Pretreatment has no effect overall, there is a less than 0.01% chance of randomly observing an this big (or bigger) in an experiment of this size. The effect is considered extremely significant.

Data analyzed: IC70s

Source of Variation	Degrees of Freedom	Sum of Squares	Mean square
Duration	1.0	88.98	88.98
Pretreatment	1.0	1266	1266
Interaction	1.0	0.2456	0.2456
Residual (error)	20.0	138.5	6.927
Total	23.0	1494	

Does Duration have the same effect at all values of Pretreatment?

Interaction accounts for <0.1% of the total variance.
F = 0.04. DFn=1 DFd=20
The P value = 0.8525
If there is no interaction overall, there is a 85% chance of randomly observing so much interaction in an experiment of this size. The interaction is considered not significant.

Does Duration affect the result?

Duration accounts for 5.96% of the total variance.
F = 12.85. DFn=1 DFd=20
The P value = 0.0019
If Duration has no effect overall, there is a 0.19% chance of randomly observing an effect this big (or bigger) in an experiment of this size. The effect is considered very significant.

Does Pretreatment affect the result?

Pretreatment accounts for 84.75% of the total variance.
F = 182.77. DFn=1 DFd=20
The P value is < 0.0001
If Pretreatment has no effect overall, there is a less than 0.01% chance of randomly observing an this big (or bigger) in an experiment of this size. The effect is considered extremely significant.